SERDP Project CP-1243

Development of Spatially-Based Emission Factors from Real-Time Measurements of Gaseous Pollutants Using Cermet Sensors

SERDP Final Sponsor Report

Energy Systems Division
Argonne National Laboratory

ARGONNE IS OPERATED BY THE UNIVERSITY OF CHICAGO FOR THE U.S. DEPARTMENT OF ENERGY OFFICE OF SCIENCE

THE UNIVERSITY OF CHICAGO

Report Documentation Page

Form Approved
OMB No. 0704-0188

1. REPORT DATE	2. REPORT TYPE	3. DATES COVERED
MAR 2005		**00-00-2005 to 00-00-2005**

4. TITLE AND SUBTITLE	5a. CONTRACT NUMBER
Development of Spatially-Based Emission Factors from Real-Time Measurements of Gaseous Pollutants Using Cermet Sensors	5b. GRANT NUMBER
	5c. PROGRAM ELEMENT NUMBER
6. AUTHOR(S)	5d. PROJECT NUMBER
	5e. TASK NUMBER
	5f. WORK UNIT NUMBER
7. PERFORMING ORGANIZATION NAME(S) AND ADDRESS(ES) **Argonne National Laboratory,Energy Systems Division,9700 South Cass Avenue,Argonne,IL,60439**	8. PERFORMING ORGANIZATION REPORT NUMBER
9. SPONSORING/MONITORING AGENCY NAME(S) AND ADDRESS(ES)	10. SPONSOR/MONITOR'S ACRONYM(S)
	11. SPONSOR/MONITOR'S REPORT NUMBER(S)

12. DISTRIBUTION/AVAILABILITY STATEMENT
Approved for public release; distribution unlimited

13. SUPPLEMENTARY NOTES

14. ABSTRACT

15. SUBJECT TERMS

16. SECURITY CLASSIFICATION OF:			17. LIMITATION OF ABSTRACT	18. NUMBER OF PAGES	19a. NAME OF RESPONSIBLE PERSON
a. REPORT **unclassified**	b. ABSTRACT **unclassified**	c. THIS PAGE **unclassified**	**Same as Report (SAR)**	**65**	

About Argonne National Laboratory

Argonne is operated by The University of Chicago for the U.S. Department of Energy Office of Science, under contract W-31-109-Eng-38. The Laboratory's main facility is outside Chicago, at 9700 South Cass Avenue, Argonne, Illinois 60439.For information about Argonne and its pioneering science and technology programs, see www.anl.gov.

Availability of This Report

This report is available, at no cost, at http://www.osti.gov/bridge. It is also available on paper to U.S. Department of Energy and its contractors, for a processing fee, from:

U.S. Department of Energy
Office of Scientific and Technical Information
P.O. Box 62
Oak Ridge, TN 37831-0062
phone (865) 576-8401
fax (865) 576-5728
reports@adonis.osti.gov

SERDP Project CP-1243

Development of Spatially-Based Emission Factors from Real-Time Measurements of Gaseous Pollutants Using Cermet Sensors

SERDP Final Sponsor Report

Prepared by

Principal Investigators:
Dr. Laura Skubal, Dr. Michael Vogt, and Dr. Natalia Meshkov

Energy Systems Division
Argonne National Laboratory

Submitted to:

Robert W. Holst, Ph.D.
SERDP/ESTCP
901 N. Stuart Street Suite 303
Arlington, VA 22203-1821

March 2005

Table of Contents

List of Acronyms used in this report

AA	atomic absorption spectroscopy
ABS	acrylonitrile-butadiene-styrene
AC	Alternating Current
ANL, Argonne	Argonne National Laboratory
ANN	artificial neural network
CEM	continuous emissions mMonitoring
CNN, NN	Computational Neural Networks
COTS	commercial off the shelf
CTR	Center for Transportation Research (a DOT facility at ANL)
DC	direct current
DETF	Diesel Engine Testing Facility
DoD	Department of Defense
DOE	Department Of Energy
DOT	Department of Transportation
EFs	emissions factors
EG	error goal
EPA	Environmental Protection Agency
FDM	fused deposition modeling
GC/MS	gas chromatography/mass spectroscopy
GRNN	General Regression Neural Network
LED	light emitting diode
MSA	Method of Standard Additions
MSATs	mobile source air toxics
NIST	National Institute of Standards and Technology
PNN	probabilistic neural network
ppb	parts per billion
ppm	parts per million
ppmv	part per million by volume
RBFN	Radial Basis Function Network
RP	rapid prototyping
SC	spread constant
SEM	scanning electron microscopy
SERDP	Strategic Environmental Research and Development Program
SLA	stereolithography
SVM	support vector machine
TICs	toxic industrial chemicals
TiO_2	titanium dioxide
UATs	urban air toxics
UV	Ultraviolet
WBO	tungsten bismuth oxide
YPG	Yuma Proving Ground
YSZ	yttria-stabilized zirconium oxide

List of Figures

List of Tables

Acknowledgements

The investigators and authors would like to extend their appreciation and acknowledge SERDP for funding this research, and thank Dr. Robert Holst for his support during this project. We would also like to thank Mr. Charles Botdorf for volunteering the use of Yuma Proving Ground for this project, Mr. James Minich and Mr. Richard Voogd for their engineering efforts, Mr. Joe Gregar for experimental apparatus constructed, and Drs. Victor Maroni and Bryan Splawn for performing microscopy during the course of the project.

Executive Summary

The United States Military will eventually need to satisfy federal pollution emissions regulations during training exercises with stationary and mobile diesel-based equipment. Currently, the Environmental Protection Agency (EPA) supports the computation and use of emissions factors to estimate pollutant emissions for nearly all types and sources of pollution, such as stationary diesel generators and mobile vehicles, and scale them up to represent large activities such as military training maneuvers and facility operations (EPA AP-42). An emission factor is a representative value that attempts to relate the quantity of a pollutant released to the atmosphere with an activity associated with the release of that pollutant. Emission factors are generally used to estimate emissions from a source when more reliable emissions data, such as records from continuous emission monitoring (CEM) or from stack tests are not available for that source. For many urban air toxics (UATs) and mobile source air toxics (MSATs), the EPA lacks ambient air toxic concentration data. Data has been collected is non-temporal, non-spatial, and cannot be used for emission factors. Because of this, emissions factors often require significant overestimation.

The development of emissions factors (EFs) could be improved significantly. Reliable EFs could reduce the need for gross overestimation if individual source emission characterizations supporting the EFs could be improved using non-permanent, on-location CEM technology. A new characterization technique was needed to produce "instantaneous" pollutant concentration profiles of emissions from both stationary and mobile sources. The instruments needed to be portable and capable of detecting both low and elevated concentrations of pollutants. The research presented in this report was intended to support the need to identify and characterize emissions of trace air toxic compounds, especially persistent organic pollutants, from operations and activities at Department of Defense (DoD) facilities. The compounds targeted for this study included acetaldehyde, acrolein, benzene, and 1,3-butadiene. These toxics contribute significantly to UATs and MSATs.

An instrument was developed that was self-contained, person-portable, and capable of being operated from a notebook computer, providing near-real-time emissions analyses. The instrument employed inexpensive, nearly disposable, miniature sensor arrays capable of rapidly detecting and characterizing air toxics in real time. Sensing elements in the array were composed of various ceramics, metals, and metal oxides tailored to be sensitive to specific compounds. The arrays were self-heated to an ideal operating temperature, and were then exposed to the four primary compounds of interest, at different concentrations and in different combinations, in air and mixed into actual diesel exhaust. Chemical "signatures" were gathered and recorded, and a library of signatures was constructed.

The sensing array used two different types of sensing elements, *voltammetric* and *photocatalytic* sensing elements, and two different chemical measurement techniques to improve chemical detection and discrimination. Both are experimental technologies with the voltammetric technique being the more mature of the two. Voltammetry is normally an analysis technique applied to aqueous systems. Voltammetry used in this project was tailored specifically for gas

detection. The voltammetry proved capable of detecting a wide range of gas concentrations, from part per million levels to percent levels. Software was developed to implement voltammetry at near-real-time speeds. Efficient and flexible chemometrics methods (neural nets and support vector machines) were used to resolve composite signals, effectively allowing gas concentrations to be determined. The more novel photocatalytic microsensors demonstrated far lower power consumption and at ambient temperatures than the voltammetric sensing elements did. The photocatalytic microsensors produced meaningful signatures to some of the target analytes at saturated concentrations, but were not able to measure target gases at ppm levels. The voltammetry-bases measurement technique coupled with the photocatalytic sensors required more development than this program allowed, so the use of the photocatalytic microsensors was discontinued.

Results from this work demonstrated that the instrument could be used to detect and discriminate the four gases of interest at varying low (ppm) concentrations. The microsensors created in this research could readily be tailored for detection of other toxic industrial chemicals at part per million levels. Additional effort is needed to improve sensor detection at low part per billion levels. That effort may include the use of a gas pre-concentrator (increasing sensitivity by increasing the effective surface area of the sensors) and/or introducing nanoparticle films to increase sensor reactivity to target gases.

Projects prior to this SERDP effort explored other sensor applications where ppb levels of detection were not required. These included the detection of insect pest (termite) infestations, detection and classification of fires (on board naval ships), and detection and classification of weapons of mass destruction (cyanide compounds and TICs). The significant advancement of this sensing technology made during the course of this project will allow all of these applications to be readdressed and solved. Demonstrations of that capability are underway at the time of this report.

Objective

This project responded to the need to identify and characterize emissions of trace air toxic compounds, especially persistent organic pollutants, from operations and activities at Department of Defense (DoD) facilities. The project had three main objectives: (1) development of field-portable CEM instrument (miniature sensors and arrays) capable of detecting and characterizing trace air toxic compounds rapidly in near-real-time; (2) integration of pollutant-data collection into spatial and temporal emission profile models of pollutants and correlating these with specific DoD activities; (3) development of improved emission factors for the targeted pollutants released during various activities. The emission factors and the quantifiable estimates of their uncertainty were to be incorporated into a structured, verifiable, user-friendly model. Project deliverables were to be new toxic gas CEM instrument, an emissions model for mobile and stationary emissions sources, and a software tool for calculating EPA-approved emission factors.

The first of the objectives was accomplished. Gas microsensors and arrays were fabricated and new electronic instrument was built and tested against the gases of interest during several series of experiments. A significant portion of the second objective was accomplished by completing a large portion of the field testing in a special-purpose Diesel Engine Test Facility (DETF) in Argonne's Center for Transportation Research. Testing at the DETF greatly reduced project expenses and allowed the project to advance despite a funding reduction during the second year. Using the DETF, a library of chemical composition signatures was developed for acetaldehyde, acrolein, benzene, and 1,3-butadiene in air and in diesel exhaust at several different concentrations and in a wide range of combinations. The project was discontinued by SERDP before the second objective (field testing at Yuma Proving Ground) was finished and before the third objective (emission model and emissions factors) could begin.

Background

A new characterization technique is needed to produce "instantaneous" emission pollutant concentration profiles from both stationary and mobile sources. The instruments must be portable, capable of detecting both low and elevated concentrations of pollutants, and engineered to provide CEM. Characterization of gaseous emissions in-situ will allow for improved emissions factors that can be computed for future pollution management.

Emissions Factors

Currently, the EPA lacks ambient air toxic concentration data for most of urban air toxics (UATs) and mobile source air toxics (MSATs) (listed in Tables 1 and 2 of the Strategic Environmental Research and Development Program Statement of Needs for FY2002 *http://www.serdp.org/o2SONJ/CPSON-0201.html*). Data that has been collected is non-temporal and non-spatial, and cannot be used for emission factors.

Emission factors are used to develop estimates of pollutant emissions for essentially all types and sources of air pollution (EPA AP-42). Consequently, emission factors play an important role in planning and implementing many air pollution control programs. An emission factor is a representative value that attempts to relate the quantity of a pollutant released to the atmosphere with an activity associated with the release of that pollutant. Emission factors are usually expressed as the weight of pollutant divided by a unit weight, volume, distance, or duration of the activity emitting the pollutant. Emission factors are used to estimate emissions from all major types of air pollution: point (large stationary), area, mobile, and biogenic sources (e.g., trees). In most cases, these factors are averages of all available data of that has been quality assured for facilities in the source category. Emission factors are generally used to estimate emissions from a source when more reliable emissions data, such as monitoring data from continuous emission monitoring (CEM) or from stack tests are not available for that source.

Gas Detection

Instruments to support CEM and improve the modeling of emissions factors begin with gas sensors. In recent years, much effort has been devoted to developing technologies to facilitate the detection and analysis of gaseous organic pollutants. Traditional gaseous organic analyses usually rely upon collection and sorption of the gaseous organic onto a fiber, transport of the fiber to a laboratory, desorption of the organic from the fiber, and analysis by gas chromatography/mass spectrometry (GC/MS). Although good detection limits and speciation can be achieved with GC/MS analysis of the samples, the sample collection process is lengthy, complex, and the analytical portion rarely can be performed in situ. Analytical technology is moving toward a more "instantaneous" approach, where an instrument can be used in-situ to produce immediate contaminant concentration profiles. The use of solid state sensors aligns with this approach.

Metal oxide semiconductors have been found useful as gas sensors for gases such as O_2, CO_2, H_2O, NO, NH_3, CH_4, alcohols, etc. The most extensively studied oxides for this purpose are

ZnO and SnO_2 (Henrich and Cox 1994). Application of metal oxides as gas sensors exploits the change in surface conductivity that occurs when gas molecules are adsorbed at the oxide surface. When the change in conductivity is large enough to be measured, it can be used to monitor the presence of the gas molecule. Sometimes certain metals deposited on the oxide surface enhance the sensitivity and selectivity of oxide sensors.

The ANL voltammetric and photocatalytic microsensors are active chemical measurement devices (Bard and Faulkner 1980) that also are metal-oxide enhanced (Kumazawa 1999). They are comprised of a miniature electrochemical cell sensing element (< 1 cm^2) and control software to produce a virtual instrument. Both devices generate a complex and unique electrical signature when excited by a varying electrical potential while being exposed to chemical analytes (Edmonds 1988).

In a voltammetric cell, the analytes react (oxidize or reduce) at very characteristic potentials according to the following simplified equation (Smyth and Vos 1992):

$$Ox + ne^- \Leftrightarrow Red \qquad\qquad Red + X \Leftrightarrow Ox + Y \qquad (1)$$

Ox = oxidizing species, Red = reducing species

In a catalytic reaction, a reversible reduction is followed by regeneration of the electroactive species. The resultant voltammogram is very effective at fingerprinting compounds and mixtures (Radomski et al. 1995 and Salikhdzhanova et al. 1994). The electrochemical cell can be driven to react by the applied potential or the cell can produce a current-limited steady state output potential that follows the Nernst equation (Fraden 1993):

$$E = Eo + ((RT)/nF)\ln(C_O/C_R) \qquad (2)$$

C_O: concentration of oxidant, C_R: concentration of reduced product, n: number of electrons transferred, F: Faraday constant, R: gas constant, T: absolute temperature, E_O: electrode potential at standard state. Nernst equation governs many half-cell reactions in electrochemical cells.

The cell/sensor can operate in either mode. A microcontroller driving the measurement is programmable and allows the output to be an analog value for interfacing to control equipment, or it can be a classification and confidence factor for reporting to a monitoring system.

The ANL devices have been under development for a variety of military applications that range from low-level human metabolic gas monitoring (breath analysis for diving applications) to intelligent fire detection systems (distinguishing complex burning mixtures). All the components have been commercially manufactured for military testing and evaluation in live demonstrations. The prototype systems use popular and inexpensive commercial-off-the-shelf (COTS) support electronics and communication follows popular industry standards. The analysis software employs a collection of digital filters and neural networks to identify the signatures. This approach also allows unknowns to be classified and re-recognized in the future.

There has been some interest in investigating TiO_2 in sensor applications and the photocatalytic gas sensor investigated for this project employs that material. Titanium dioxide has been useful as an oxygen sensor because at high temperatures oxygen diffuses into its oxygen vacancies, increasing its resistivity (Sharma et al. 1996). At low temperatures, chemisorption of gases at the

oxide particle surface changes surface states and charge distribution of the oxide with concomitant change in resistivity (Edelman et al. 2000). In metal oxide sensors the oxides are usually deposited on a substrate in either thin (50 to 200 nm) or thick (0.02 to 10 mm) films. Thin films of metal oxide semiconductors such as TiO_2 either in single phase or in combination with other oxides have been studied as gas sensors. For example, recent investigations address novel nanostructured materials such as TiO_2, and WO_3 in single phase or as mixed oxides (Comini et al. 2000 [1]), and TiO_2-Fe_2O_3 thin films. These applications exploit semiconductor-sensing properties based on surface reactions between the semiconductor and the gases in the atmosphere, which cause a change in the semiconductor's resistance due to charge transfer between the adsorbate and the adsorbent. Two types of reactions have been shown to occur: with the oxygen absorbed at the surface, or directly with the semiconductor surface (Comini et al. 2000[2]). Stability, porosity and high surface to volume ratio are key properties for a sensing film. The sensing properties are enhanced with decreased particle size of the semiconductor. TiO_2 thin films with different dopants were successfully used to detect ppm levels of alcohol at 400 to 500°C (Sberveglieri et al. 2000). TiO_2 thin films prepared using a chemically modified sol-gel technique produced anatase particle sizes of 3 to 30 nm and greatly increased sensitivity to ethanol and methanol detection at 400°C to 500°C compared to standard sol-gel methods which produce larger (25-50 nm) particle sizes (Garzella et al. 2000).

Several recent studies involving TiO_2 thick-film sensors have focused on nanometric oxides for atmospheric CO detection (Traversa et al. 2000, Carotta et al. 1999, Carotta et al. 2000). TiO_2 particle sizes ranged from 10 to 60 nm in these studies. The sensors were deployed at 450°C. It was found that smaller particle size greatly enhanced the sensor sensitivity. TiO_2 has also been used recently in a novel method for detecting alcohols and aromatic compounds. There, it was found that when AC voltage was applied to the sensor, the resulting conductance, surface potential and phase lag could be used to distinguish various compounds (Islam et al. 1998; Kumazawa et al. 1999). It was also found that illumination with monochromatic light (700 nm wavelength) improved the sensitivity of the sensor (Kumazawa et al. 1999). However, none of the above studies with the TiO_2-based sensors intentionally exploited the photocatalytic properties of this semiconductor.

TiO_2 has long been known as an effective photocatalytic agent for removing organic pollutants from both aqueous and gaseous environments. Heterogeneous semiconductor photocatalysis relies upon the use of photoactive semiconductors, such as TiO_2, to not only adsorb noxious and pollutant gaseous emissions, but to photocatalytically oxidize (or reduce) them into less toxic organics and carbon dioxide (CO_2). When TiO_2 is illuminated with light of energy equal to or exceeding its bandgap energy (3.2 V [volts] for anatase TiO_2), electrons are excited into the conduction band creating positive holes in the valence band. If these electron-hole pairs do not recombine to produce heat, they can promote oxidative and reductive electron transfers as described in the simplified Equations 3 through 8 (Butler and Davis 1993, Das et al. 1994, Luo and Ollis, 1996, Serpone and Pelizzetti, 1989)

$TiO_2 - h\nu \rightarrow h^+ + e^-$	electron-hole pair formation	(3)
$e^- + M^{(n+1)} \rightarrow M^n$	reduction	(4)
$h^+ H_2O_{(ads)} \rightarrow \bullet OH + H^+$	oxidation of adsorbed water	(5)
$h^+ + 2OH^-_{(ads)} \rightarrow \bullet OH^+ OH^-$	oxidation of adsorbed hydroxide ions	(6)

$$\bullet OH + R \rightarrow R\bullet + H_2O \quad \text{propagation} \quad (7)$$

$$R\bullet + O_2 \rightarrow R2 + HO_2 \quad \text{termination} \quad (8)$$

where $h\nu$ = light energy, h^+ = hole, e^- = electron, M^n = oxidized compound, R = reduced aldehyde, alcohol, light hydrocarbon, aromatic, chlorinated solvent, etc. and R2 = oxidized R.

Photoexcited electrons can reduce compounds sorbed onto TiO_2. Generally, holes do not directly oxidize organic compounds. Instead, they react with adsorbed water molecules or hydroxyl ions to produce hydroxide radicals, powerful oxidizing species that in turn oxidize sorbed species (described by the mechanisms in Equations 5 through 8).

A variety of gases have been detoxified by TiO_2 photo-oxidation. Included in these are benzene, toluene, acetaldehyde, trichloroethylene, formaldehyde, propionaldehyde, pyridine, ethylene, and acetone (Buechler et al. 1998, d'Hennezel and Ollis 1997; d'Hennezel, et al. 1998; Hager and Bauer 1999; Jacoby and Nimlos 1996; Maira et al. 2000, Sampath et al. 1994, Sirisuk et al. 1999, Sopyan et al. 1994, Takeda et al. 1995). Detoxification processes occur by the sorption of the gas upon the TiO_2 followed by ultraviolet light (UV)-induced photooxidation. Results from these studies have shown conversions up to 100% (d'Hennezel and Ollis 1997).

Several studies have taken this phenomenon one step further to detect atmospheric constituents based on TiO_2 sorption processes in the presence of light. Distinct conductivities and surface potentials are produced when thin-film rutile TiO_2 is exposed to vaporized liquids such as methanol, ethanol, n-pentanol, benzene, toluene, and monochlorobenzene in darkened conditions. These responses are greatly enhanced when the TiO_2 is exposed to these constituents and illuminated with 700 nm light (Kumazawa et al. 1999). In another study, rapid responses in photoconductivity occurred when TiO_2-Nb was exposed to oxygen pressure changes. These responses were obtained at 120°C, a temperature much lower than most metal oxide sensors require for operation (Golego et al. 2000).

In a recent ANL study (Skubal et al. 2000), thick-film anatase TiO_2 sensors were developed that operated at room temperature and photocatalytically responded to a variety of organic gaseous constituents. The investigation employed a systematic approach to analyze resistance signatures from anatase TiO_2 sensors, enabling investigators to distinguish and profile individual gaseous constituents. The "smart" microsensors and processing capabilities allowed investigators to extract complex information that normally was not taken advantage of with chemical sensors. Electrical perturbations including actual peak applied potential, average applied potential, applied potential rate change, and applied potential waveform shape (stair-step, square wave, differential pulse) were implemented using programmable microcontroller devices. Sensor responses (select or all) to an analyte, temperature, light, electrical perturbations, etc. were combined into a surface or hypersurface that provided the signal processing with a wealth of information to support the identification, differentiation, and quantification of a gaseous [analyte] constituent. Experimental results indicated that the TiO_2 sensors showed promise as viable sensors capable of distinguishing different contaminants by providing characteristic and reproducible electrical signals for each compound tested. Distinct characteristic responses were obtained to different gases (isopropanol. ethanol, and xylene in ppm concentrations) when sensors were illuminated with UV light at room temperature. Tests also indicated that the sensors were reusable and reproducible. These results can be explained by the photocatalytic

properties of TiO_2 exploited in previous ANL investigations (Meshkov et al. 1999; Skubal et al. 1996; Skubal, 1999; Skubal et al. 2000) and outlined in equations 3 through 8 above. Illumination induced reactions in the adsorbed gases leading to changes in the electrical properties of the TiO_2. Humidity found in ambient room air provided the water/hydroxyl groups sorbed to the TiO_2 and needed to produce radicals upon illumination. The molecules sorbed to the surface of the TiO_2 were photochemically transformed, released, and the process repeated continuously.

Other previous investigations at ANL had shown that certain organic compounds exhibited a specific affinity for TiO_2, and allowed varying amounts of charge transfer to occur between TiO_2 and sorbed compounds. Functional groups on a compound dictated the orientation of the sorbed compound to the TiO_2, the binding of the compound to the TiO_2, and the pathway for charge transfer to occur from the TiO_2 to the sorbed compound. Different functional groups affected the interaction of the compound with the TiO_2. This had been confirmed by experimental results, and was used as the basis for developing sensor selectivity. Investigators found that results from the sensor were reproducible, consistent, and that the sensor could be reused without thermodynamic or chemical regeneration before reuse. From an economic standpoint, it was advantageous to have a sensor that was self-cleansing/self-regenerating in the presence of ambient air.

Materials and Methods

The experimental characterization of DoD-produced emissions required the selection of a subset of Toxic Industrial Chemicals (TICs) found in diesel exhaust and the design and fabrication of a specialized instrument to support CEM of those gases.

Primary Focus on Four Diesel Exhaust Gases: Benzene, 1,3-Butadiene, Acetaldehyde, and Acrolein

After an assessment of expected atmospheric contaminants at Yuma Proving Grounds (the DoD field test facility collaborating with ANL on this project), the investigators decided to focus primarily on gases inherent in diesel exhaust. The project scope of work was tailored to focus on four significant mobile source air toxics at YPG from diesel exhaust gases: acetaldehyde, acrolein, benzene, and 1,3-butadiene. Table 1 lists selected information about these gases. Source concentrations of these diesel constituents, especially from older engines, typically is in the several hundred parts per million range (Stern 1968).

Target Toxic Gases in Diesel Exhaust

EPA has very little data regarding the concentrations of acetaldehyde, acrolein, benzene, and 1,3-butadiene released from stationary and mobile diesel exhaust sources. The experimental stage of this project would provide valuable data needed by EPA. Table 1 presents information on the compounds of interest.

Table 1. Selected Information on Diesel Exhaust Gases

	Acrolein, C_3H_4O	Acetaldehyde, C_2H_4O	Benzene, C_6H_6	1,3-Butadiene, C_4H_6
Molecular Weight	56.06 g/mol	44.05 g/mol	78.11 g/mol	54.09 g/mol
Conversion factors	1 ppmv = 2.33 mg/m^3 1mg/m^3 = 0.43 ppmv (20^oC and 1atm)	1 ppmv = 1.83 mg/m^3 1 mg/m^3 = 0.55 ppmv (20^oC and 1 atm)	1 ppmv = 3.25 mg/m^3 1 mg/m^3 = 0.31 ppmv (20 ^oC and 1 atm)	1 ppmv = 2.25 mg/m^3 1 mg/m^3 = 0.44 ppmv (20 ^oC and 1atm)
OSHA TWA limit (8-hour day, 40-hour week)	0.1 ppm	200 ppm	10 ppm	1 ppm
*EPA ambient concentrations in suburban areas (1988 data)	No data	1.63 ppbv	1.27 ppbv	0.67 ppbv
Combustion related vehicular			75-270 ppmv	

emissions**				
*EPA average concentrations released from 1981-1989 year cars	No data	0.804 mg/mile	10.214 mg/mile	1.405 mg/mile
Comments	breaks down fairly rapidly in the air (half-life about 1 day) by reacting with other chemicals	atmospheric half-life is 15 hours, reacts with hydroxyl radicals	reacts with other chemicals in the air and breaks down within a few days	breaks down quickly in air by sunlight, half-life is 2 hours to a few days depending on the amount of sunlight.

* Source: *EPA Motor Vehicle-Related Air Toxics Study*, April 1993, EPA 420-R-93-005
** Source: *Air Pollution volume III, Sources of Air Pollution and Their Control*, A. Stern, ed., Academic Press, NY 1968.

Target Detection Limits

An instrument was designed and developed to detect 1 ppm to 1000 ppm of the four constituents, and to achieve a detection limit of 1 ppm or less. The choice of this detection limit was based on the feedback the project investigators received from EPA indicating that a rapid, portable, and inexpensive sensor capable of detecting in the low ppm range would be very useful as a screening tool, would have a potential for wide-range applications, and would be the most valuable to the EPA.

Contact was established with Mr. John Bosch of EPA, who had expressed a strong interest in this project and its ongoing progress. Contact was also established with Mr. Joe Sumers at the EPA Transportation Laboratory in Michigan. They both promised to provide the project staff with further information on desirable detection limits for sensor development.

Initial detection levels for the instrument were planned for ppm ranges, but approaches were investigated that would allow the instrument for this project to be refined to achieve lower than ppm levels of detection as well. The most feasible improvements were planned to be introduced with each new generation of instruments.

Part Per Billion Detection Limits

Although ppb levels of detection were not desired by EPA, strategies were refined in case other interested groups required lower characterization levels. Several approaches were available to lower the detection limits of the project instrument and are described as follows.

1 Use existing microsensors. Current results indicate that testing should be able to achieve at least a 0.1 ppm detection limit with current voltammetric microsensors without any further modification. Staff can easily perform tests at these concentration levels with the available equipment.

2 Concentrate samples with a resin trap. Tenax traps can be used to capture components in a pre-measured volume of sample gas and then be treated to release those trapped components into a smaller volume. This effectively increases the concentration. Concentrated samples are desorbed from the resin and pumped into the sensor chamber for detection. A simple calculation based on time and flow rate will enable our system to back-calculate the concentrations. This is an established technique for laboratory analyses. The benefits are increased sensitivity without changes to the remainder of the instrument. The costs are added complexity to the final instrument and delays in response time.

3 Increase the contact area between the detector and the gases. One way to accomplish this is by increasing the size of the detector (sensor). The project's current sensors are approximately 0.64 cm^2.in area. It was shown in past experiments that if the surface area of the sensors is increased to 6.4 cm^2, the detection limit will increase tenfold as well (the measurable current is a function of exposed surface area). Sensitivity also can be improved by introducing new materials to the sensor, using alternative sensor fabrication techniques, or increasing the gas-sensor interface area and the number of grain boundaries at those interfaces (the location where the gases react). This can be accomplished by using nanometer diameter particles rather than the micrometer diameter particles that are currently used. Fabrication methods for nanoparticles are still experimental, and require additional investigations, but a series of nanoparticle voltammetric microsensors were fabricated for this program and will be characterized as funding and time allow.

4 Improve measurement technique. Square wave voltammetry can be implemented instead of the triangular sweep (cyclic) voltammetry currently being used. The voltammetry technique used for gas detection in this project is based upon voltammetry used for aqueous electrochemistry. Square wave voltammetry greatly improves the detection limits of and response speed for aqueous constituents. As such, it should be able to be adapted for gas detection in a similar way that the linear sweep voltammetry was used. Square wave voltammetry applies a changing differential potential and takes twice as many measurements as an equivalent linear sweep voltammetry. The technique is designed to apply opposite polarities at each given potential value. The difference between the polarities corrects for the charging capacitance current, isolates the Faradaic (the chemical reaction) signal from the capacitive charging portion of the current, and effectively eliminates the "noise" that can mask the chemical reaction. The improvements are two-fold: much faster response times (0.25 second sweep times vs. 20 second sweep times) and much lower detection limits made possible by a far better chemical signal-to-noise ratio. This method has been implemented and demonstrated, but requires further investigations to characterize it as a replacement for the existing linear sweep voltammetry.

Instrument Development

In FY2003, a new version of the sensor equipment was fabricated and field tested as a portable instrument to characterize diesel emissions produced by stationary and mobile sources. In the new version hardware and software were improved. Methods to both identify and quantify gas analytes were developed.

Hardware

The instrument was an evolution of existing gaseous voltammetry equipment developed at Argonne. The instrument was minimized onto a single electronics chassis. All sensing arrays can be run and the data from them processed using a notebook computer.

Photocatalytic and Voltammetric Sensors

Two types of sensors, photocatalytic and voltammetric, were fabricated and evaluated for inclusion in the final emissions instrument, as shown in Figures 1a and 1b.

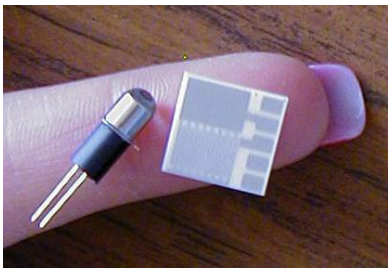

Figure 1a. Photocatalytic Sensor and the UV Diode Light Source

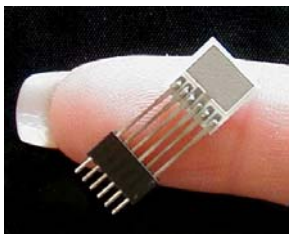

Figure 1b. Voltammetric Sensor

Photocatalytic sensors are based on the photocatalytic properties of metal oxide semiconductors. They grew out of Argonne's research in photocatalytic systems focusing on using TiO_2-assisted photocatalytic oxidation and reduction processes for environmental applications. The basic principle underlying photocatalytic redox reactions is as follows. Upon illumination with ultraviolet light, electrons are promoted from the valence band to the conduction band in TiO_2, leaving holes in the valence band. Both electrons and holes are free to react with constituents sorbed to the TiO_2 surface. The extent of interaction with the surface depends upon the chemical properties of the sorbed gaseous constituent. Reaction of the gas with the TiO_2 surface affects the conductivity of the TiO_2 surface which can be measured. Figure 1a shows the photocatalytic sensor and the UV-emitting diode used with it as the excitation source. Figures 2a and 2b show the assembly containing the photocatalytic sensor and the light source mounted inside a tube allowing gases to flow through it.

Three types of photocatalytic microsensors were fabricated in the sensor laboratory, each employing different forms of TiO_2, and using different geometries: Degussa P25 TiO_2 (primarily the anatase crystal structure), rutile TiO_2, and nanoparticle TiO_2 (nanoparticles were synthesized through the controlled hydrolysis of titanium tetrachloride in our laboratory). Platinum electrodes were screen-printed onto an aluminum oxide (Al_2O_3) substrate, fired at 1300°C to sinter into a thick film, and tested for conductivity. The TiO_2 powder was mixed with an electronic vehicle (special organic viscous base) into a paste, which was then screen-printed on top of the inter-digitated platinum electrodes and fired at 320°C.

The photocatalytic sensor apparatus was reduced in size from approximately 1 ft^3 to approximately 3 in^3 by incorporating a miniature high-intensity ultraviolet (UV) light emitting diode (LED), comparable in size to the sensor, to replace the external UV reactor as a light

source to induce photocatalytic reactions. A new miniature test chamber has been prototyped to support the operation (Figure 2b).

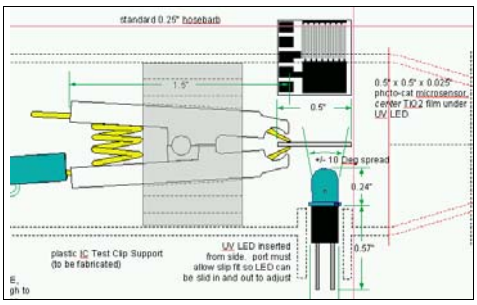

Figure 2a. Photocatalytic Sensor Assembly Design

Figure 2b. Photocatalytic Sensor Assembly Prototype

Voltammetric sensors (shown in Figure 1b) exploit the oxygen ion transport properties of solid electrolytes to detect and identify gases that are oxidized or reduced at electrode surfaces. A solid electrolyte is sandwiched between platinum electrodes as shown in the micrograph below (Figure 3).

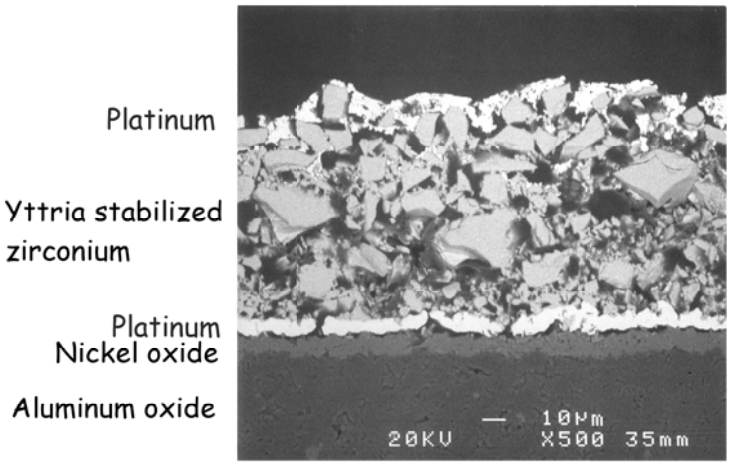

Figure 3. Voltammetric Gas Microsensor Film Cross-Section

The sensor is exposed to a gas sample, a voltage (usually of saw-tooth form) is applied to the electrodes, and the current response is measured. A voltammogram - a graph displaying the current versus voltage - is collected. A typical 6-cycle voltammogram is shown in Figure 4.

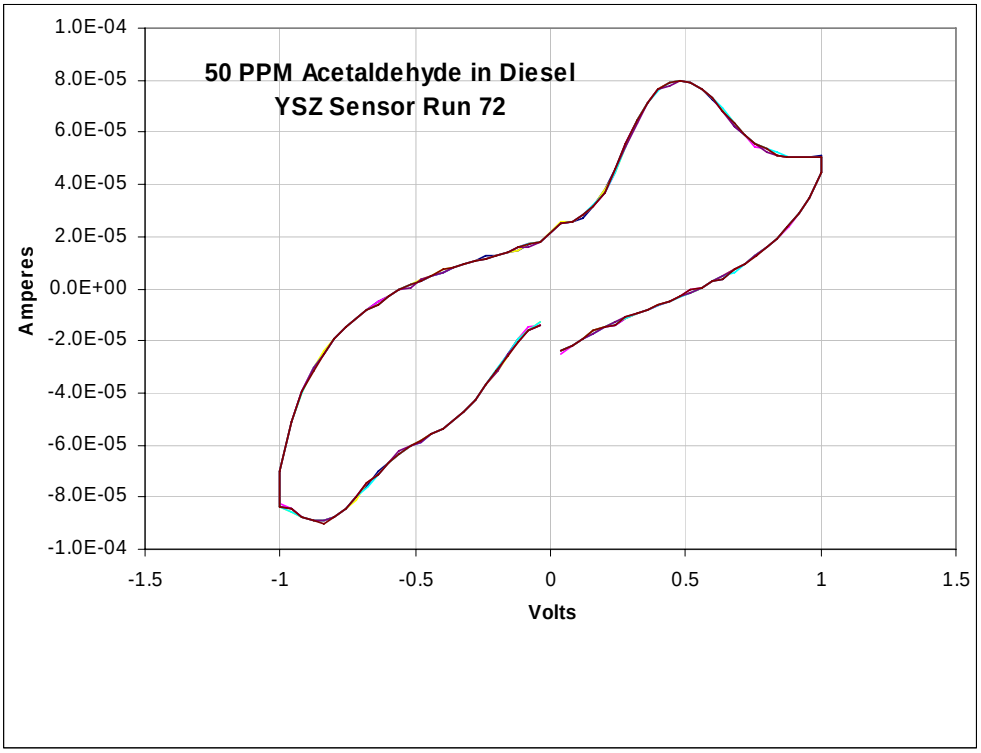

Figure 4. Sensor Signal Reproducibility.
A YSZ sensor was exposed to 50 ppm acetaldehyde in diesel exhaust. Six voltammograms were collected and are displayed. As shown, reproducibility is excellent, as the voltammograms are indistinguishable from each other.

The shape of a voltammogram will depend on the composition of the gas sample measured, and on individual component concentrations. Typically, as the voltage increases, the current increases slowly until the voltage approaches the redox potential of the gas. At that point the current increases sharply because more ions are made available for carrying electrical current. As the gas at the electrode surface becomes depleted and the applied potential changes, the current lessens and a current peak is observed. When the applied potential is reversed, a similar pattern repeats itself in reverse. Other factors influence the shape of the voltammogram in addition to the redox potential of the sample gas and its concentration. These factors include multiple reactions, reversibility of the reactions taking place at the electrode, and the electrolyte used. Two kinds of electrolytes have been used in the voltammetric sensors for this project:

1. Yttrium stabilized zirconium microparticles (YSZ sensors)
2. Yttrium-stabilized zirconium doped with tungsten bismuth oxide microparticles (WBO sensors)

In the experiments, described later, the two voltammetric sensors (YSZ and WBO) were at first used individually. Later, the two sensors were assembled in a mini-array, and used simultaneously to produce a composite response.

Initial Focus on the Photocatalytic Sensors

During the initial stages of this project, sensor development focused on advancing the photocatalytic microsensors to the maturity level of the voltammetric microsensors. Their potential for operation at ambient temperatures without the need for self-heating made them attractive for field-portable, long-term CEM applications. During the year FY2002 experiments were performed involving several gases (ethanol, isopropanol, methylene chloride, xylene, and acetone) at their saturation points. Specific gases triggered distinct responses from the photocatalytic sensor. Conductance/impedance spectrums for different gases varied both in magnitude and in shape in response to the applied voltage. The micro-sized UV diode has been shown to be effective in producing the photocatalytic response in TiO_2 and is capable of replacing a much larger UV reactor.

During FY2003 similar impedance tests were performed with the TiO_2 photocatalytic sensors on the target diesel exhaust gases. However, the responses to the target gases were below existing measurement instrument resolution. These results shifted the project direction to using the more mature, responsive voltammetric sensors on exhaust streams, until improvements could be made to the photocatalytic measurement technique.

Programmable Potentiostat Instrument

Project staff worked with ANL's Computer and Information Systems Division to improve components of the existing voltammetry instrument, and to collect the components into a single chassis to produce a field-portable system. The designs went through two generations of testing and integrating components. The voltammetry system produced is unique in that it is designed to accommodate gaseous analytes, not liquid ones as all existing commercial voltammetry systems are designed to analyze. Fabricated project voltammetric systems are shown in Figure 5a, 5b, and 5c. The chassis, power supply, and temperature controller are commercial components; the potentiostat voltammetry electronics are specialize ANL-developed components.

Figure 5a. Generation II Integrated Electronics External Front

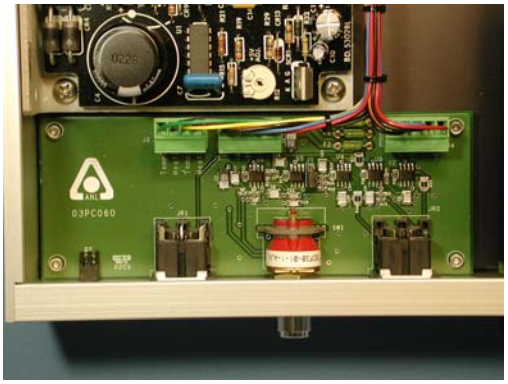

Figure 5b. Generation II Integrated Electronics Chassis

Figure 5c. Generation II Field-Portable Gaseous Voltammetry Instrument

During the project, improvements were made to components and the overall system. The system will continue to be miniaturized and diversified for more flexible use.

Microsensor Enclosures

In order to convert the laboratory sensor array to an array suitable for field use, the sensing elements/arrays needed to be contained in a protective enclosure (Figure 6). Rapid prototyping (RP) methods were employed for this engineering and fabrication need. Two different RP fabrication methods were employed: stereolithography (SLA) and fused deposition modeling (FDM). Three different types of plastic materials were used in the RP models: Watershed™, ABS, and polycarbonate.

The case/enclosures were designed to allow gases to flow over the sensor surfaces while protecting them from direct physical contact. The RP fabrication is very efficient and supports continual engineering upgrades following each generation of field testing. The initial designs do not include internal baffles or injection ports for calibration and validation testing, but instead allow behavior studies to be made to evaluate the different plastic materials to determine which, if any, produces an interfering signal via off-gassing of the plastic exposed to the heated sensor/array surface. It was expected that some detectable level of off-gassing would be present and tests to determine compensation procedures were completed. Similar enclosures were fabricated using Pyrex glass to help determine optimal geometry and to establish the level of chemical interferences given from the plastics.

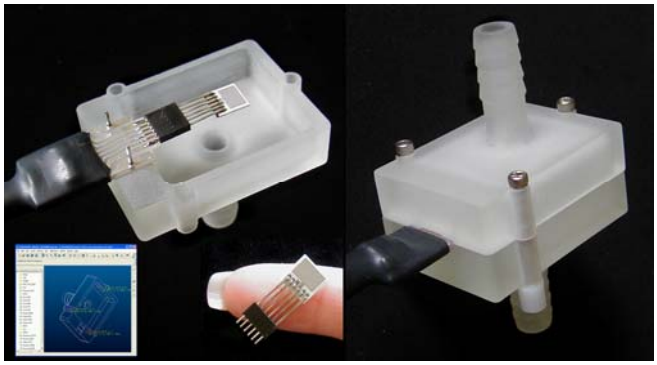

Figure 6. SLA-Fabricated Sensing Element Enclosure Made with WaterShed™ 11120

The details of the methods used are only tangential to this report and are included in the Appendix.

Software

Specialized software plays a role in both operation of the instrument and in analysis of the acquired chemical signatures. For this project, all software was developed in the MathWorks MATLAB™ environment to promote flexible operation and easy adoption of the developed instrument. MATLAB was selected as a development environment for the instrument for several reasons. Software tools exist to significantly streamline complete instrument and system development, including the Excel Builder, Curve Fitting Toolbox, Embedded Target for Motorola microcontroller, a Neural Network Toolbox, and recently an experimental Support Vector Machine Toolbox. A more detailed explanation of the MATLAB environment is included in the Appendix.

Several algorithms were developed for both data acquisition and for signature analysis. These algorithms were tested using both synthetic response data and the voltammograms gathered during the experimentation.

Voltammetry Measurement

Routines to implement both linear sweep voltammetry and square wave voltammetry were developed and tested during the extensive experimentation efforts. The linear sweep voltammetry produced simpler to interpret semi-quantitative results and was employed for the majority of the experiments as it provided detailed chemical signals corresponding to the underlying electrochemical reaction behavior. The much faster square wave voltammetry was tested for speed and sensitivity improvement over linear sweep voltammetry: both of these features improved significantly, but at a cost of significantly greater chemical “noise”. Square wave voltammetry produces higher sensitivities and sampling rates that are desirable in a final instrument, and will be pursued as noise masking, filtering, and cancellation techniques are refined.

Signature Analysis

Several parametric and nonparametric chemometric methods were available for performing more complex curve fits, or function approximations, along high numbers of dimensions. For this work, a General Regression Neural Network (GRNN) algorithm was employed. These topics are introduced here, and are described in detail in the Appendix.

Computational Neural Networks

A neural network is inspired by and loosely models the architecture and information processing capability of the biological brain (Masters 1993). An Artificial Neural Network (ANN) accomplishes this by simulating each biological neuron with an integrated circuit as a collection of gates and transistors while a Computational Neural Network (CNN) accomplishes this through execution of a series of computer instructions. Neural networks can be structured to perform classification (Raimundo and Narayanaswamy 2001), to approximate equations (Joo et al. 2001), and to predict values (Freeman and Skapura 1991, Winquist et al. 1993).

Radial Basis Function Networks

Radial Basis Function Neural Networks (RBFNs) are effective for classification problems, and employ a layer of radial basis function neurons that effectively represent a "library" of known chemical signatures. This layer accepts voltammogram signatures as patterns and performs a Bayesian (Marcelloni 2001) nearest neighbor classification (Beebe et al. 1998) of the patterns to produce a match, along with an associated confidence measure for that match. This type of NN algorithm was used to establish initial discrimination capability of the instrument, identifying and classifying the components in the experimental mixtures of the four target gases. A test matrix was compiled with fixed-concentrations (100 ppm of each component) in combinations of one, two, and three gases added to the diesel exhaust background. All gas mixtures from the diesel mixture test matrix were classified correctly. Other methods for classification were also investigated to set the stage for more complex discrimination problems.

Probabilistic Neural Networks

A Probabilistic Neural Network (PNN) is an extension to the RBFN that introduces statistical weighting for the given classification categories based upon the occurrences and classes of the example signatures in the training collection. While training samples for a RBFN are selected by the developer from a population of samples expected to represent the desired classes, the samples for a PNN are drawn randomly from that same collection. It is anticipated that if a particular sample is popular across a collection, then examples of that will occur more often in a training set, and this will be realized as additional neurons in the selection layer. When an example of a popular sample is presented to the NN for processing, it will produce a stronger response than a less popular example. In this way, a-priori statistical information for the entire population is captured in the classification process and used to improve class assignment. PNNs were tested for use with the voltammograms gathered during the discrimination experiments. The PNNs also produced zero straight-classification error (straight classification meaning only that no value analysis was performed, only simple assignment of signatures to categories) and as such were uninteresting to compare to the RBFN classifier performance.

Generalized Regression Neural Networks

The General Regression Neural Network (GRNN) is also a specialized version of the RBFN, but includes a linear output layer that allows weighted combinations of analog values to be produced. GRNNs are specifically tailored for regression or function approximation and allow input patterns to be mapped to scalar or vector values. By training a GRNN with different voltammograms gathered during experiments that exposed the sensing array to varying concentrations of one or more components, the functional relationship between the changing voltammograms and the concentration values is modeled and captured in the network weights. This effectively "calibrates" the network algorithm and allows unknown voltammograms to be analyzed for concentration data, interpolating values in between known training samples.

For this effort, several different GRNN architectures were implemented to analyze entire input voltammograms for individual target components – producing a single scalar value, and to extract multiple components simultaneously. A collection of the individual component analyzers is more complex than the single GRNN "to extract all components" network, but both performed well and produce very low level error when validated against known samples removed from the original training data.

A GRNN with a more complex architecture was used to produce discrimination and concentration values from tests with gas mixtures. This algorithm was trained to detect a given single value of 100 ppm concentrations of each of the four target toxic gases. When the trained network was presented with mixtures of these gases, it recognized the presence of any of the four gases responding within 25% of the 100 ppm target values. This algorithm structure correctly classified all combinations of the four target gases in a diesel background, singly, in pairs, and in triples. Additional test will be completed to establish discrimination of individual gases at varying concentrations for each component. (Detailed results of the performance of the neural network classification and analysis methods can be found in the Results section of this report.)

Support Vector Machines

Support Vector Machines are classification and regression algorithms that are derived from the field of statistical learning theory. They often can be simpler in structure than an equivalent neural network algorithm performing the same task, but have advantages of being both more economical computationally and are based upon provable operations vs. the black-box neural network methods. SVM have been adopted for chemometrics applications and were investigated for analyzing our voltammetry data.

We found that the performance difference between the properly tuned GRNN function approximation and the SVM approximator were minimal, and did not warrant the adoption of the SVM signature processing at this time. Future experimental results may require the improved generalization that the SVM is theoretically capable of, so these algorithms will remain as a tool evaluated and ready to apply as needed.

Diesel Engine Test Facility Replaces Portions of Field Testing

The original Experimental Plan anticipated field testing of the developed instruments, both to benchmark the equipment and to begin to gather representative measurements from various diesel emissions sources. Two issues altered that strategy – a reduction in the second year's funding, and, the availability of the diesel test engines at Argonne's Department of Transportation's Advanced Engine Test Facility. Due to the availability of this facility the project was able to perform many tasks at Argonne that were originally planned for Yuma Proving Ground. The Test Facility contains a variety of diesel engines, operated at specific loads and with specific fuels that can be selected and controlled. This facility, for both light-duty and heavy-duty engine research, allowed the project to generate emissions and test them both with experimental microsensors and with gas chromatography/mass spectrometers in situ. Exhaust parameters in this facility can be controlled by adjusting inputs into the engines. In a field environment, select organic diesel exhaust gases of interest (such as our target gases) occur in the presence of all other gases from diesel exhaust. Using this facility offset expenses and eased the transition from laboratory research to field demonstrations.

Gas Characterization Procedures and Verification Methods

Gas species and mixture characterization methods were developed for the project's experimental CEM instrument. The detection method developed for use in the field was validated in the laboratory using defendable common laboratory methods.

Traceable Gas Characterization Procedure

Diesel exhaust was pumped at known flow rates through a mixing chamber where it was spiked with known and certified concentrations of acetaldehyde, acrolein, benzene, and 1,3-butadiene (the 1 ppmv, 10 ppmv, 100 ppmv, and 1000 ppmv gas standards were National Institute of Standards and Technology (NIST)-certified concentrations and were procured through AGA, Inc.). Flow rates of the spiking gases were measured on calibrated and certified flow meters from ScienceWare™, Inc. The initial diesel exhaust was checked for concentrations of acetaldehyde, acrolein, benzene, and 1,3-butadiene via GC/MS. The final mixed results did not require GC/MS re-verification because the concentrations of the spiking gases were known, the flow meters were calibrated, and both were certified by NIST.

Diesel Sampling Procedure

Diesel exhaust was collected at ANL's Transportation Center Diesel Engine Test Facility using 37.7 liter Tedlar™ sampling bags and Teflon fittings. Samples were transported between buildings and analyzed within minutes to hours of sampling using the experimental voltammetry instrument.

GC Verification

Ambient acetaldehyde, acrolein, benzene, and 1,3-butadiene concentrations were determined in the exhaust using a Hewlett Packard HP5971 Quadrapole™ Gas Chromatograph/Mass Spectrometer (GC/MS) with a 30 meter DB-5 0.25 μm film (thickness) column. 300 μL of exhaust was injected into the GC/MS for each experiment. The total run time was 7 minutes at

35˚C (isothermal). Acetaldehyde eluted at 1.22 minutes; 1,3-butadiene at 1.31 minutes; acrolein at 1.46 minutes; and benzene at 2.59 minutes. Approximate detection limits are: benzene, 1 ppm; 1,3-butadiene, 1 ppm; acrolein, 2 ppm; and acetaldehyde, 20 ppm (masked by carbon dioxide).

Predicting Missing or Unknown Initial Concentrations - Method of Standard Additions

The detection method developed for the series of gas voltammetry tests included a modified version of the Method of Standard Additions (MSA). The MSA approach was ideal because responses from individual gases in a voltammogram are not as easy to predict as they are with liquid species. The MSA method is used to determine a particular component's contribution to a combined signal for a given mixture. When the individual component cannot be isolated from a mixture or compound, then a sample is 'spiked' with several predetermined amounts of that same component and the sensor response for each is recorded. The response curves for each spiked sample should follow the same governing function and when that curve is fitted, the sensor response value for a spike of "0" can be calculated. The sensor response curve to the differential samples is linear. This spike of 0 is actually the Y-intercept for the $y = mx + b$ equation. While it is convenient from a computational perspective to have a purely linear fit, it is not required – as long as the response curve is regular and can be fit, then any regular expression can be used to predict the spike=0 response. Thus the original contribution (concentration) of the target component can be calculated.

Initial tests with raw diesel exhaust were performed without the availability of a gas chromatograph/mass spectrometer (GC/MS) instrument to analyze the composition. Four target gases were selected that were of importance to DoD and EPA. These gases were acetaldehyde, acrolein, benzene, and 1,3-butadiene. It was anticipated that these would be in very low concentrations as produced from a well-managed experimental diesel engine test stand. Spike amounts of each component (from the certified stock gas standards) were introduced into diesel samples. Both the un-spiked and spiked samples were used to produce voltammograms from an array that contained two materially-different types of microsensors.

The common MSA was modified to allow for an entire 100-point voltammogram to be used for each signal value. This presented a problem as the shape-change of a voltammogram is not simple and is not necessarily linear, so a simple linear curve fitting approach was not appropriate. Another issue of concern in a non-linear complex curve fit is that only the relative concentration-response values can be measured – not absolute values. This required that whatever curve fit was used, it would need to reflect the 'spike' amount, not the total amount of a chemical component.

Several parametric and nonparametric chemometric methods were available for performing more complex curve fits, or function approximations, along high numbers of dimensions. For this work, a General Regression Neural Network (GRNN) algorithm (see the Appendix for more information on Computational Neural Networks and GRNNs) was employed.

Results and Accomplishments

Engineering work was completed that produced an experimental field-portable instrument for CEM. The initial evaluations of suitable sensing array elements included both voltammetric microsensors and photocatalytic microsensors. The target sensitivity and speed were low ppm levels and near-real-time response, to satisfy EPA recommendations. This primary objective was accomplished. Much of the second objective, emissions characterization and modeling, was also accomplished through a series of emissions characterization experiments.

Photocatalytic results

Early experiments evaluating the photocatalytic sensor used an ultraviolet (UV) diode (<320 nm) to produce the excitation light source. Sensors were exposed to various gases, in the presence of the UV light and in the dark. Conductance profiles (an impedance measurement) were gathered and processed (Figure 7).

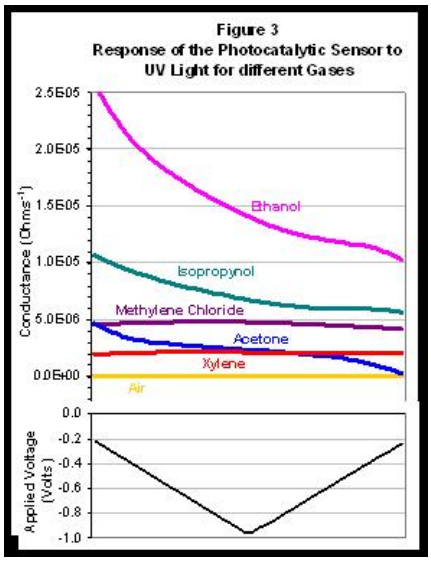

Figure 7. Photocatalytic Microsensor Responses

Figure 7 shows the response of the photocatalytic TiO_2 sensor to different gases in air when illuminated with UV light. Individual gas concentrations are at their respective saturation levels. Responses recorded are averages over six sweeps for each gas. The graph also shows the response for "uncontaminated" background air. Figure 7 illustrates the measured conductivity vs. the applied potential – the results of using the voltammetry instrument to perform impedance measurements. As Figure 7 shows, specific gases produce distinct responses from the photocatalytic microsensor. Conductances for different gases vary both in magnitude and in how they change with the applied voltage. No conductance was detected in the dark for any of the gases. Air alone exhibited no conductance either in the dark or when illuminated. The micro-sized UV diode has been shown to be effective in producing the photocatalytic response in TiO_2 and can be used to replace a much larger UV reactor. Later testing of these same gases in a diesel background indicated that the sensitivity required was not yet achievable and the

photocatalytic microsensors were discontinued for the duration of the CEM instrument development.

Voltammetric results

The prototype CEM instrument was completed using only the voltammetric microsensors and passed a series of internal electronics tests that calibrated its response to nominal target gases and established that its measurement capabilities were suitable for the emissions gas testing that would follow. Once a first prototype instrument was constructed, a second instrument was also made and evaluated using the same test procedure. The anticipated electrical current output from a voltammetric sensor was input using a calibrator and the instruments were challenged against it to establish that they would produce matching and identical results. When this was completed, the instruments were used as a pair to drive dual sensing elements as an array; one driving a YSZ microsensor and the other simultaneously driving a WBO microsensor.

The voltammetry experiments performed are listed in Table 2. The results of the emissions characterizations are shown below.

Table 2. Tests Completed with the YSZ and WBO Sensing Array

All tests were performed at a sensor operating temperature of 280˚C. Concentrations listed in this table are not detection limits, rather, they represent the wide range of concentrations typically found at a variety of diesel emission sources.

Individual gases in air: According to EPA data, concentrations of acetaldehyde, acrolein, benzene, and 1,3-butadiene range from low ppm levels to hundreds of ppms in various diesel emission sources. Since no current analytical technology can detect such a wide concentration range of these four gases, the sensor array was first tested to determine if it could detect such a span of concentrations of each of the four constituents in air without changing the sensors or operating parameters. Establishing the range of detection of these individual gases in air is important because in real world environments, source gases will be diluted with air as distance from the source increases and will span across several orders of magnitude in concentration.		
Gas tested and matrix	**Concentrations tested (ppmv)**	**Dates of testing**
acetaldehyde in air	2, 3, 4, 7, 15, 32, 67, 105, 50, 100, 200, 400, 800, 1000	9/2/03, 9/3/03, 9/24/03, 9/25/03
benzene in air	10, 50, 100, 200, 400, 800,1000	8/27/03
acrolein in air	7, 10, 35, 50, 100, 101, 148, 200, 400, 800, 1002	9/19/03, 4/10/03
1,3-butadiene in air	22, 39, 50, 59, 91, 100, 200, 400, 800, 1000	9/23/03, 4/11/03

Individual gases in a background of diesel exhaust: At a diesel emission source, the four gases of interest are in a matrix of combusted diesel fuel. Depending on the source, these concentrations can vary over several orders of magnitude. A four stroke diesel engine in ANL's Transportation Center Engine Test Facility was used to produce diesel emissions. The emissions were collected, analyzed for the four constituents by GC/MS, and spiked with various concentrations of individual gases. These tests were performed to simulate conditions found in the field, and to determine if a wide range of concentrations of the gases could be detected on a background of *diesel exhaust*.		
acetaldehyde in exhaust	1, 5, 10, 33, 50, 58, 81, 148	9/3/03, 10/15/03, 11/12/03
benzene in exhaust	8, 37, 82, 156	9/15/03, 10/15/03
acrolein in exhaust	1, 5, 10, 11, 32, 50, 59, 78	9/17/03, 10/15/03, 11/12/03
1,3-butadiene in exhaust	24, 31, 61, 102	9/22/03, 10/15/03
Mixtures of gases in a background of diesel exhaust: In real-world situations, the four gas constituents of interest exist together in diesel exhaust. The following tests were performed to determine if mixtures of constituents produced voltammograms that were distinguishable from one another, and if one gas signal dominated in the voltammograms. (In many analytical methods, high concentrations of one or multiple analytes oftentimes "swamp" the detector. This test represented the "worst case" scenario that could be found in a field application – high concentrations of analytes all competing for chemisorption/physisorption sites on the sensor).		
acrolein, acetaldehyde in exhaust	100 each	10/15/2003
acrolein, 1,3-butadiene in exhaust	100 each	10/15/2003
acrolein, benzene in exhaust	100 each	10/15/2003
acetaldehyde, benzene in exhaust	100 each	10/15/2003
acetaldehyde, 1,3-butadiene in exhaust	100 each	10/15/2003
benzene, 1,3-butadiene in exhaust	100 each	10/15/2003
acrolein, acetaldehyde, benzene in exhaust	100 each	10/15/2003
acrolein, benzene, 1,3-butadiene in exhaust	100 each	10/15/2003
acrolein, acetaldehyde, 1,3-butadiene in exhaust	100 each	10/15/2003
acetaldehyde, benzene, 1,3-butadiene in exhaust	100 each	10/15/2003
acrolein, acetaldehyde, benzene, 1,3-butadiene in exhaust	100 each	10/15/2003

Experiments began using high (1000 ppm) gas concentrations; so that determinations could be made as to whether the target gases could be detected by the voltammetric microsensors. Figure 8 shows some of the early results, and demonstrates that the four gases of interest are easily detected at high concentrations. The instrument was updated and improved to support measurements of concentrations of the same gases from low (1ppm) to high (1000 ppm) levels.

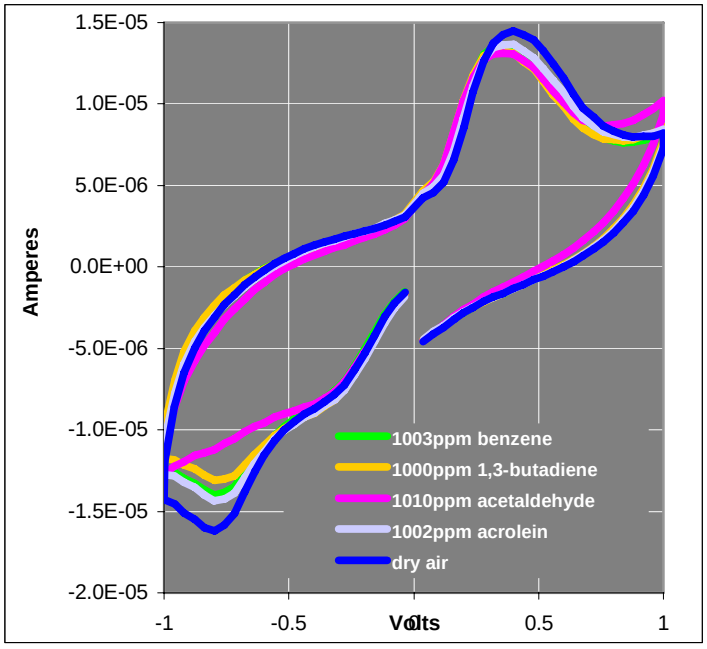

Figure 8. Diesel Exhaust Gases in Air at High Concentrations with the YSZ Sensor

The remainder of this discussion will focus on experiments performed at lower concentrations on

(1) individual gases in diesel exhaust background, and
(2) gas mixtures in diesel exhaust background.

Semi-Quantitative Analysis of Voltammetry for Detection Limits and Accuracy.
A series of experiments was performed in diesel exhaust spiked with the target gases at added concentrations ranging from 11 ppm to 156 ppm.

Figures 9 through 13 show voltammograms obtained for the four gases – acetaldehyde, acrolein, benzene, and 1,3-butadiene – in a diesel exhaust matrix at four different added concentrations of each gas (1 ppm, 5 ppm, 10 ppm, and 50 ppm) and collected simultaneously by YSZ and WBO sensors hooked up in an array. A six-cycle saw tooth voltage was applied to each sensor exposed to a particular gas, and the current responses from each sensor were measured for each cycle. The voltammograms for each of the six cycles are for all practical purposes indistinguishable, as can be seen in Figure 4. Voltammograms obtained for each cycle are then averaged over the six cycles. Each experiment was repeated seven times with both sensors for every added gas concentration and for diesel exhaust without the added gases. The seven repetitions were averaged and standard deviation was computed for each data point composing the voltammogram. The voltammograms in Figures 9 through 13 show these averages as well as the averages plus and minus the standard deviation. These graphs showing the standard deviations provide a measure of accuracy for detection of the gases at each concentration. Selected portions of the voltammograms are shown separately.

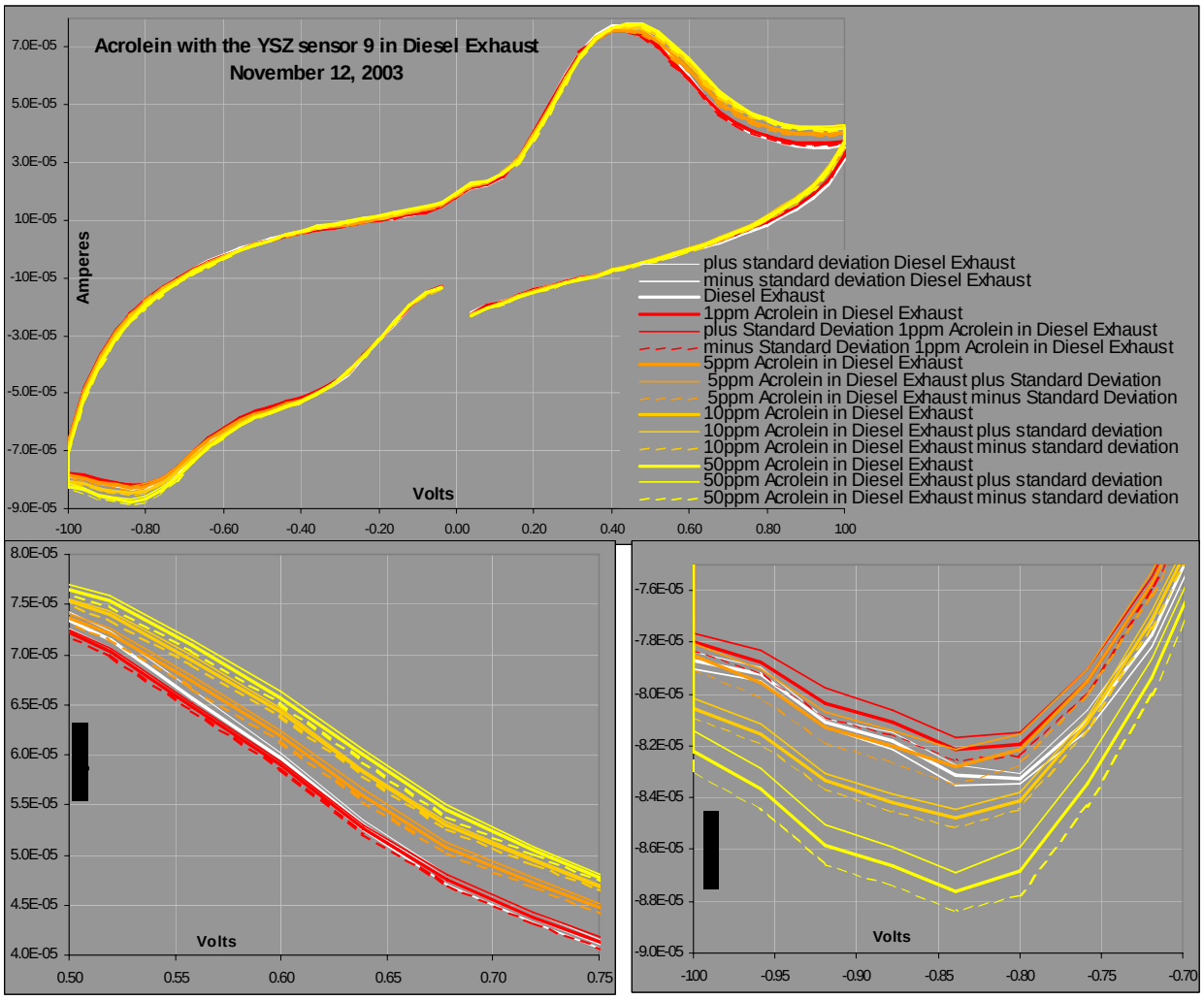

Figure 9. Acrolein on a Diesel Background - YSZ. The two bottom graphs are blown up portions of the top graph and show at which voltages the YSZ sensor is most responsive to acrolein.

Figures 9 and 10 show voltammograms obtained in a diesel exhaust matrix for acrolein. Comparison of the YSZ and WBO sensor voltammograms for acrolein leads to the following observations. We note that the portion of the voltammograms between 0.5 and 0.75 volts shows a clear separation between the four added concentrations, but the 1ppm curve is indistinguishable from the diesel exhaust background. The portion of the diagram between -1.0 and -0.7 volt shows a clear separation between the curves for 10 ppm and 50 ppm, but lower concentrations are blurred. On the other hand, the WBO sensor voltammograms appear to be more capable of discriminating lower concentrations than the higher ones. The portion of the chart for the WBO sensor between 0.6 and 0.8 volt shows a clear separation between the diesel exhaust background and the 1 ppm and 5 ppm curves, while higher concentrations overlap somewhat. In other words, WBO sensor is good at discriminating low concentrations, while YSZ is better for distinguishing higher concentrations. This is a key issue and benefit when designing a microarray instrument.

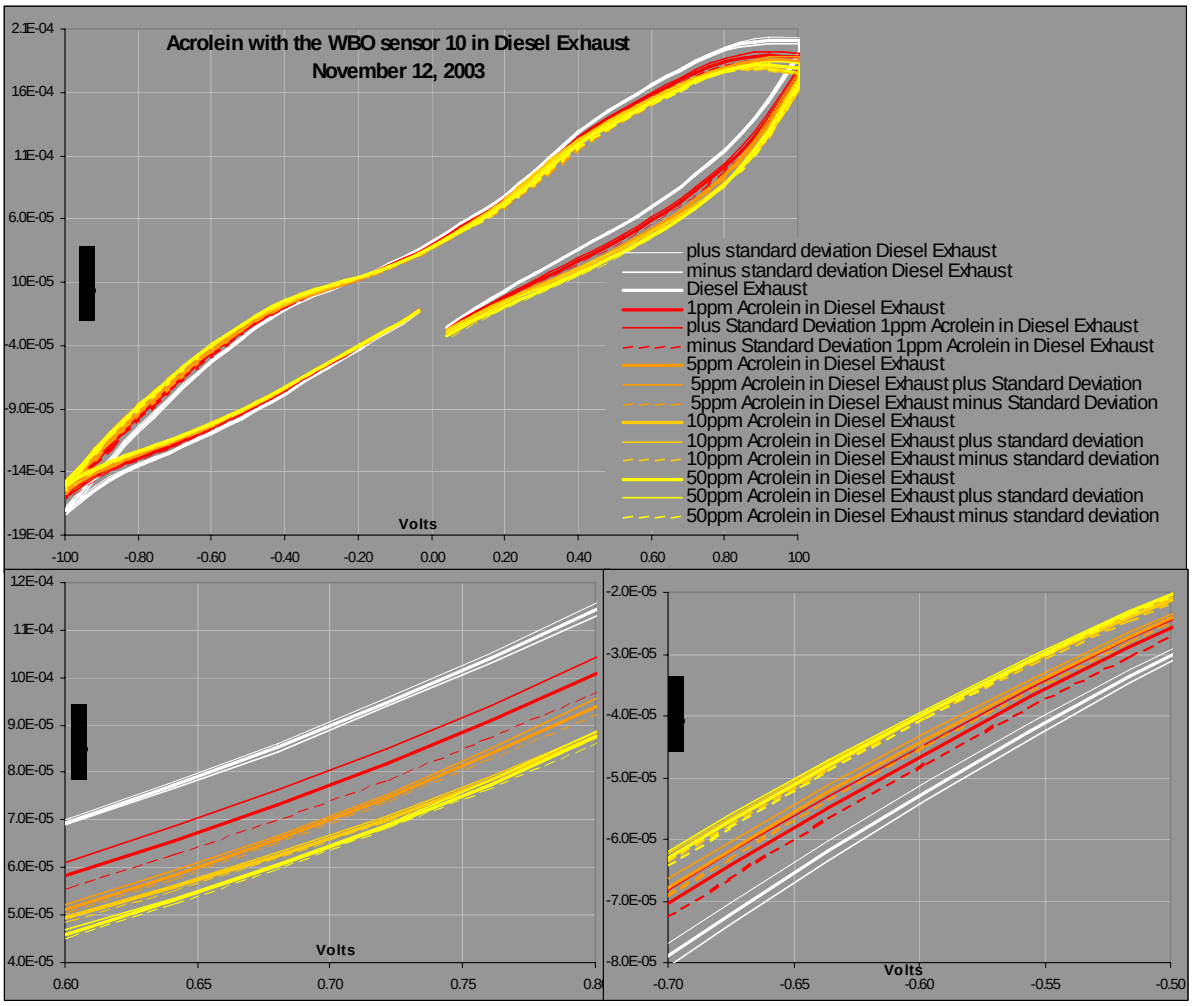

Figure 10. Acrolein on a Diesel Background - WBO. The two bottom graphs are blown up portions of the top graph and show at which voltages the WBO sensor is most responsive to acrolein.

Figures 11 and 12 show similar voltammograms obtained in diesel exhaust matrix for acetaldehyde. Comparison of the WBO and YSZ results for acetaldehyde show a pattern similar to that for acrolein, i.e. WBO appears to be better at discriminating between low concentrations of acetaldehyde than YSZ does. However, the portion of the WBO graphs between 0.4 and 0.75 volt shows a very clean separation between all the added concentrations, as well as the diesel exhaust by itself.

The graphs in Figures 9, 10, 11 and 12 clearly illustrate how two sensors in an array can complement each other by providing different signal responses to the same input.

Figures 13 through 16 show results for benzene and 1,3-butadiene in diesel exhaust at added concentrations of target gases of 1, 5, 10 and 50 ppm. For both benzene and 1,3-butadiene, the YSZ sensor results exhibit a very clear separation between the voltammograms corresponding to different concentrations, indicating that these concentrations can be clearly distinguished to within a standard deviation. On the other hand, for the WBO sensor the voltammograms for both

gases overlap for different concentrations. In addition, a wide separation between the 1 ppm and the diesel exhaust graphs suggests that much lower concentrations (0.1 ppm and below) may be detectable for these gases using the YSZ sensor.

In addition to individual gases, mixtures of gases were detected with the YSZ and WBO sensors. All gas concentrations are at 100 ppmv spikes above a background of diesel exhaust.

Table 3. Test Matrix of Multiple Constituents

Acrolein	x	x	x	x	x	x	x	x							
Acetaldehyde		x	x	x			x		x	x	x	x			
Benzene			x	x	x			x		x	x		x	x	
1,3-Butadiene				x	x	x	x				x	x		x	x

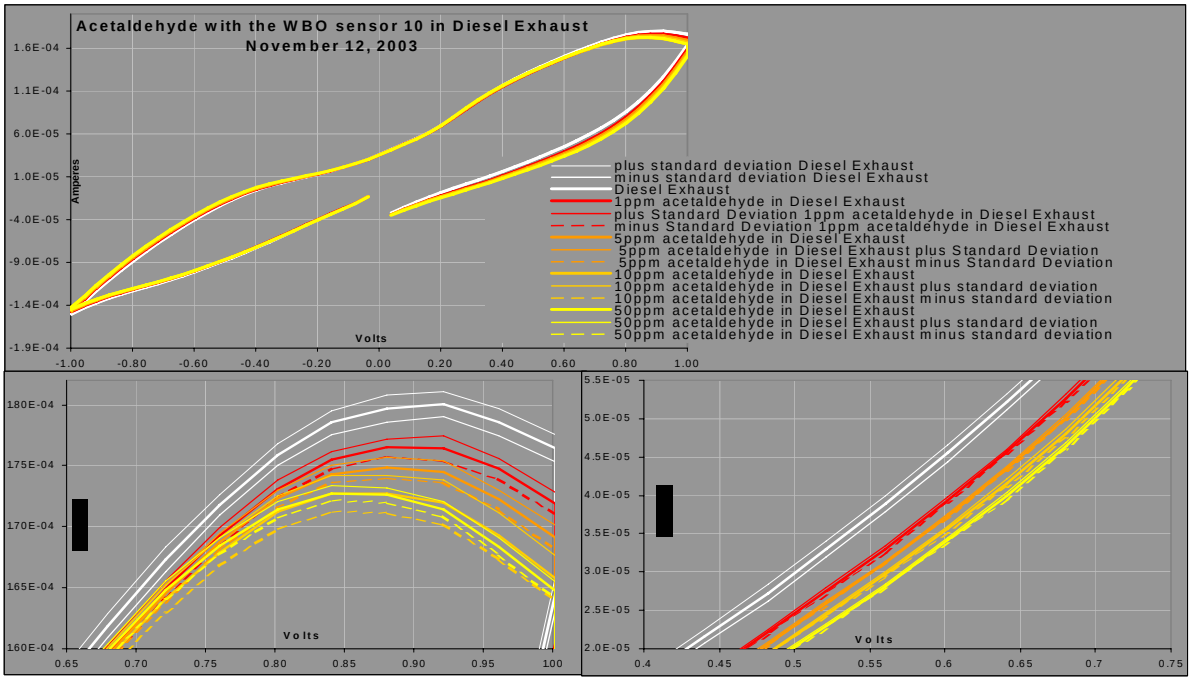

Figure 11. Acetaldehyde on a Diesel Background - YSZ. The two bottom graphs are blown up portions of the top graph and show at which voltages the YSZ sensor is most responsive to acetaldehyde.

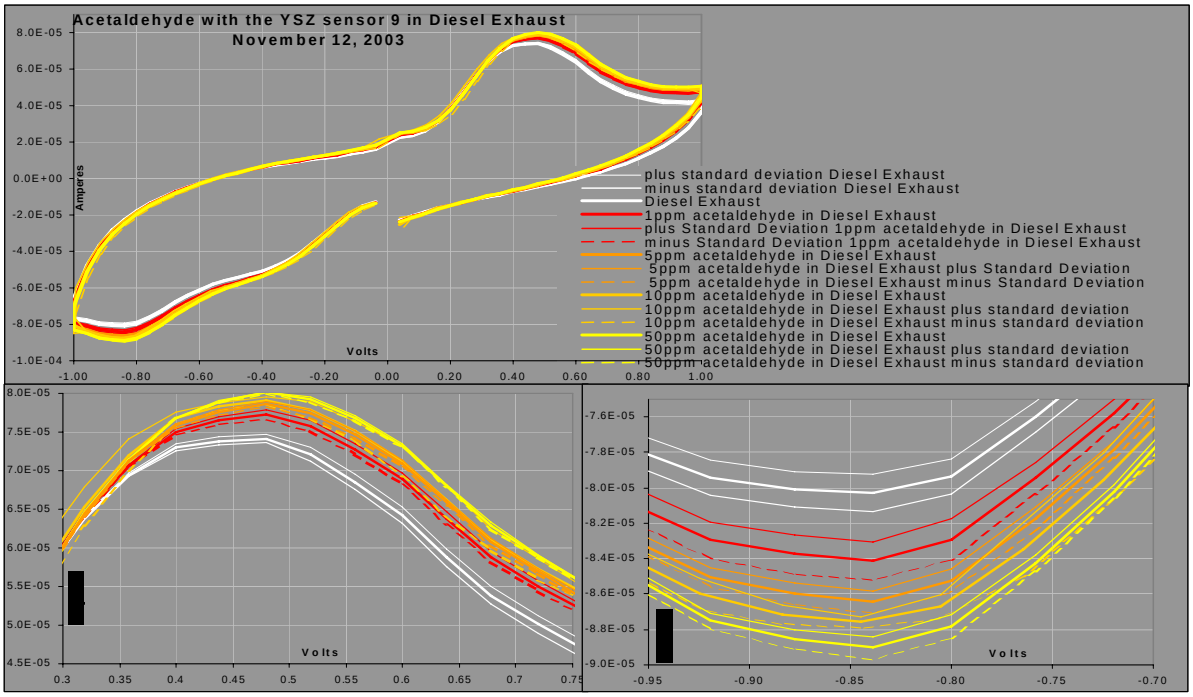

Figure 12. Acetaldehyde on a Diesel Background - WBO. The two bottom graphs are blown up portions of the top graph and show at which voltages the WBO sensor is most responsive to acetaldehyde. .

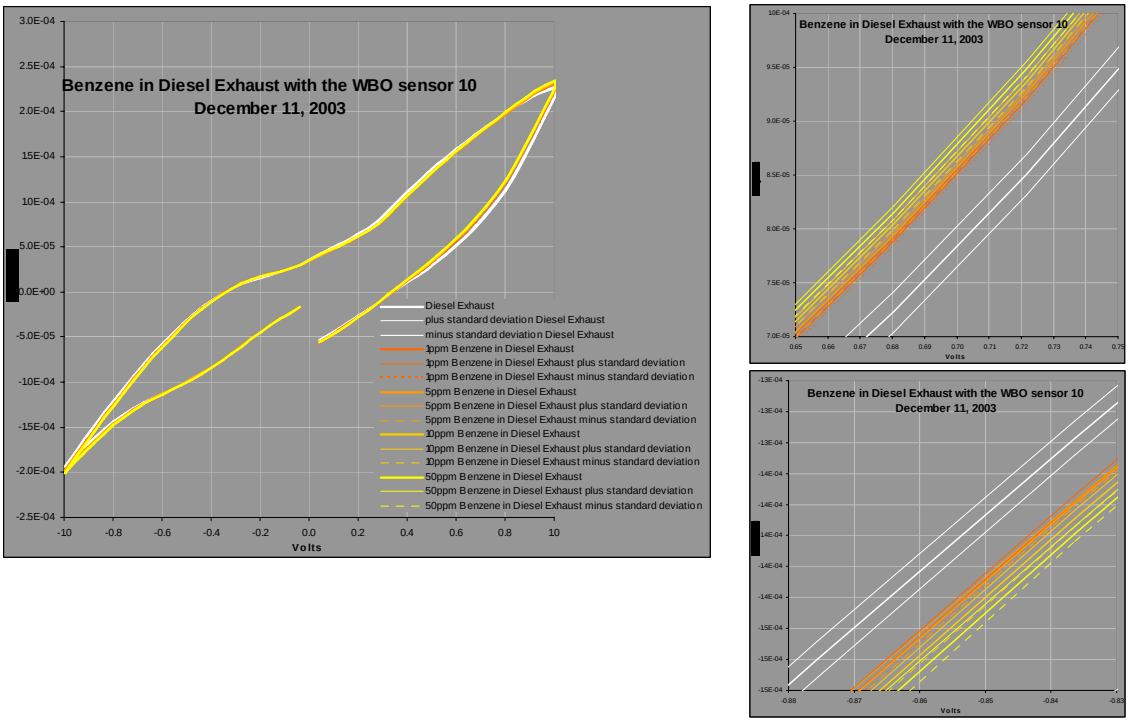

Figure 13. Benzene on a Diesel Background - WBO. The two bottom graphs are blown up portions of the top graph and show at which voltages the WBO sensor is most responsive to benzene.

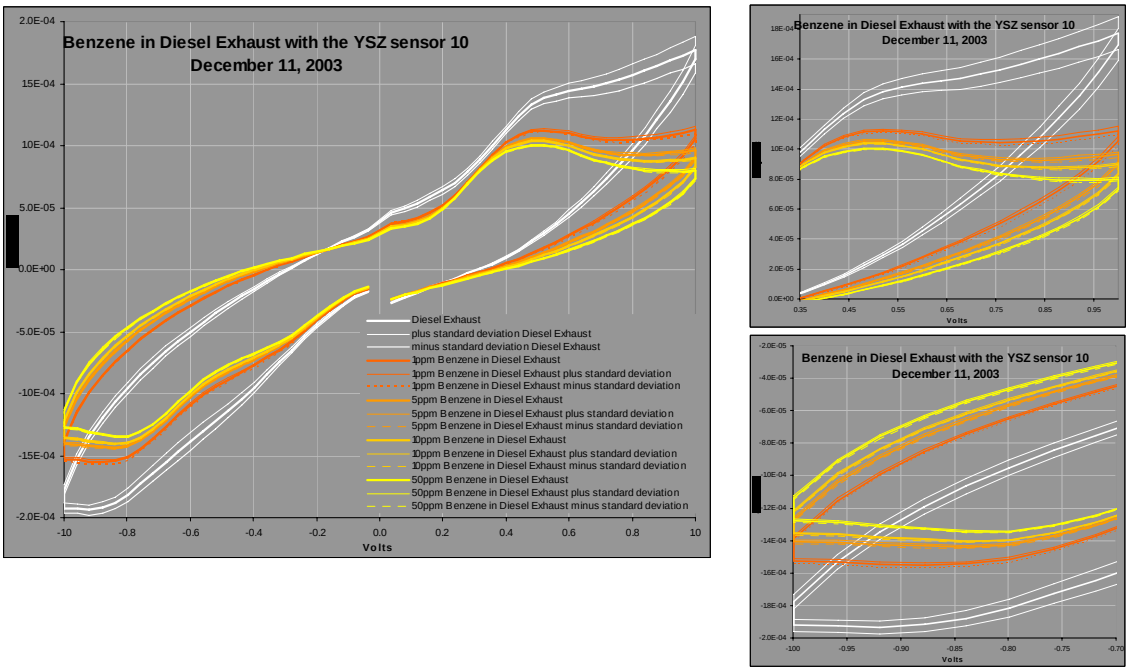

Figure 14. Benzene on a Diesel Background - YSZ. The two bottom graphs are blown up portions of the top graph and show at which voltages the YSZ sensor is most responsive to benzene.

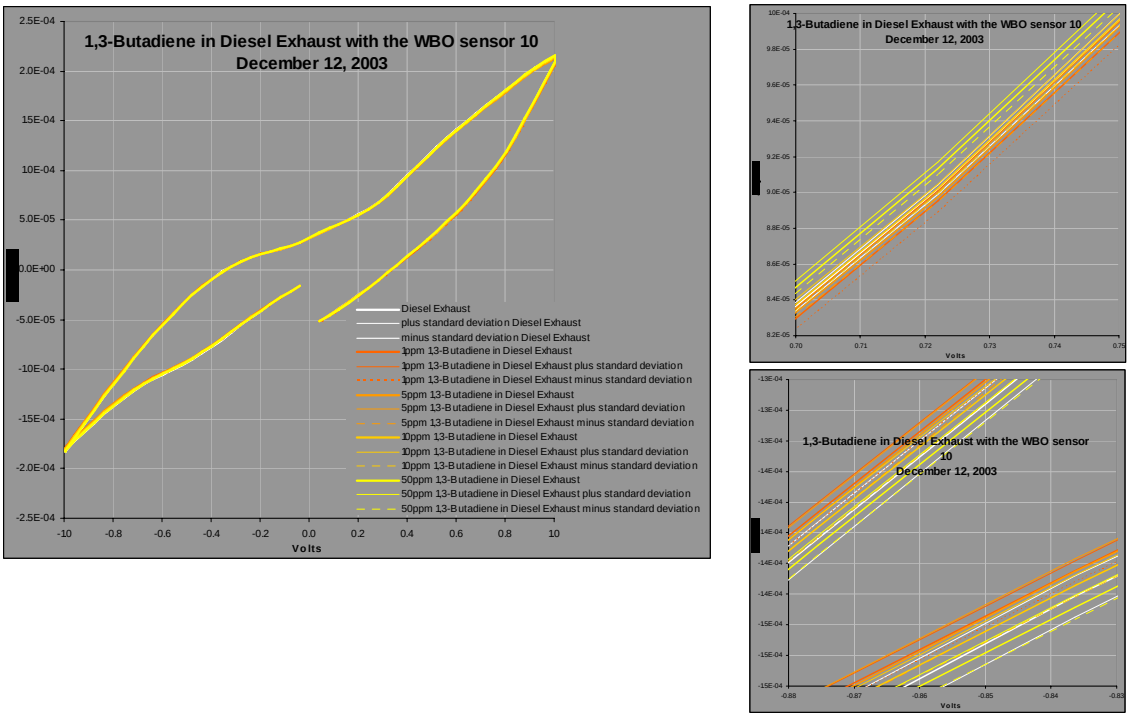

Figure 15. 1,3 Butadiene on a Diesel Background - WBO. The two bottom graphs are blown up portions of the top graph and show at which voltages the WBO sensor is most responsive to 1,3 butadiene.

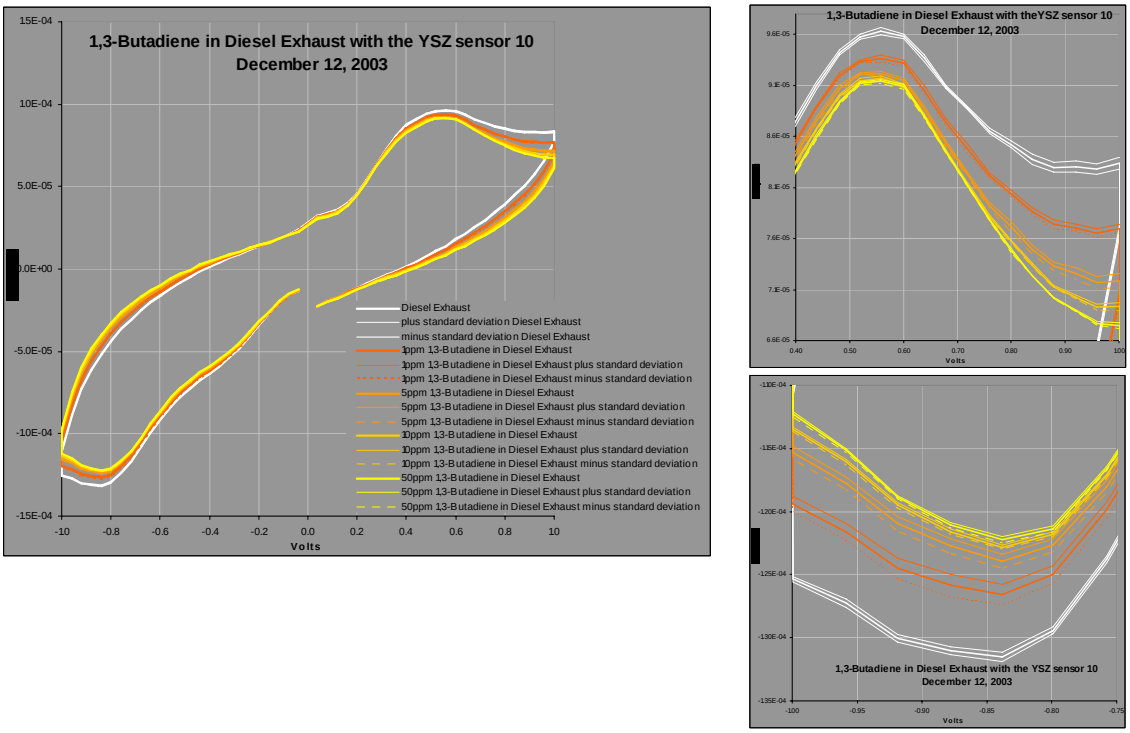

Figure 16. 1,3 Butadiene on a Diesel Background - YSZ. The two bottom graphs are blown up portions of the top graph and show at which voltages the YSZ sensor is most responsive to 1,3 butadiene.

Experiments for all four target gases in the concentration range between 10 ppm and 160 ppm exhibit distinct voltammograms for different concentrations of the same gas. Behavior of the voltammograms for a given gas changes with the concentration in a regular way for both the YSZ and the WBO sensors. These features indicate that our sensors are capable of discriminating different concentrations for these gases in the diesel exhaust matrix. Voltammograms for different gases also exhibit distinct patterns in at least one of the sensors of the array.

Voltammograms from tests in the concentration range between 1 ppm and 50 ppm show that for acrolein and acetaldehyde, the WBO sensor is good at discriminating low concentrations, while YSZ is better for distinguishing higher concentrations. However, for acetaldehyde, portions of WBO graphs show a very clean separation (well within a standard deviation) between all the added concentrations, as well as the diesel exhaust by itself. This clearly illustrates how two sensors in an array can complement each other by providing different signal responses to the same input. For both benzene and 1,3-butadiene, YSZ sensor results exhibit a very clear separation between the voltammograms corresponding to different concentrations, indicating that these concentrations can be clearly distinguished to well within a standard deviation. In addition, a wide separation between the 1 ppm and the diesel exhaust graphs suggests that much lower concentrations – 0.1 ppm and below – may be detectable for these gases using the YSZ sensor. On the other hand, for the WBO sensor, the voltammograms for both gases overlap for different concentrations.

These results clearly show that a detection limit of 1 ppm is achievable with the current instrument, and that much lower concentrations may be detectable without any significant changes. Currently established detection limits are shown in Table 4.

Table 4. Currently Established Detection Limits for Diesel Exhaust Gases with Voltammetric Sensors

	Acrolein C_3H_4O	Acetaldehyde C_2H_4O	Benzene C_6H_6	1,3-Butadiene C_4H_6
YSZ	5 ppm	1 ppm	1 ppm	1 ppm
WBO	1 ppm	1 ppm	1 ppm	50 ppm

Quantitative Detection and Discrimination Performance Analysis (CNN exercises)

The results and performance of the chemometrics methods used to quantify the capabilities of the project's developed CEM instrument are divided and described under detection and discrimination topics.

Detection Results

The Method of Standard Additions (MSA) technique described earlier in the Methods section of this report was implemented using a GRNN. This technique proved successful and will be refined for more exhaustive applications.

Implementing MSA with GRNNs

The GRNNs used were designed to accept the 100-point input and produce individual values for each spiked component. By training the GRNN with voltammograms/spike-value pairs, the network weights arrive at values that store the curve fit for the response curve of the spiking chemical. This response curve represents only the contribution of the added chemical component used for spiking, and should be independent of the other components. As may be expected, use of more spiking values leads to a better representation of the response curve, and to a more accurate curve fit. When this training stage was completed, the trained GRNN was then presented with a sample voltammogram that was produced from an analyte that was known to contain none of the chemical(s) used for the spiking.

An example of this methodology is illustrated using the WBO sensor results for diesel exhaust spiked with acetaldehyde (C_2H_4O) at added concentrations of 0, 33, 58, 81, and 148 ppm. Sextuples of voltammograms were gathered for each concentration value. The input pattern voltammograms for the 33 ppm concentration are shown in Figure 17. The resulting numerical arrays were paired up against the output target spike values as shown in Figure 18.

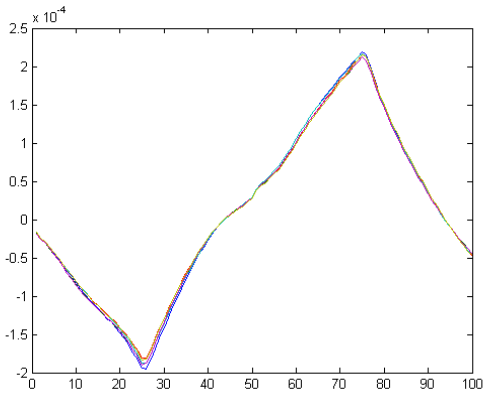

Figure 17. 33 ppm acetaldehyde–spiked diesel sextuple of voltammograms

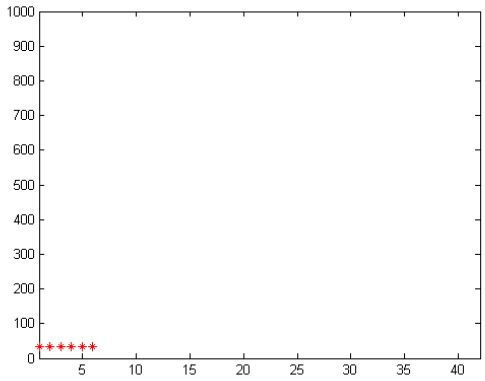

Figure 18. 33 ppm target values (calibration range of 0 – 1000 ppm)

The GRNN was trained adjusting both the Error Goal (EG) and the Spread Constant (SC) parameters until suitable curve fits were produced. The curves in Figure 19 are plots of sample concentration (ppm) on Y-axis vs. sample number along X-axis, and illustrate fit vs. sample number.

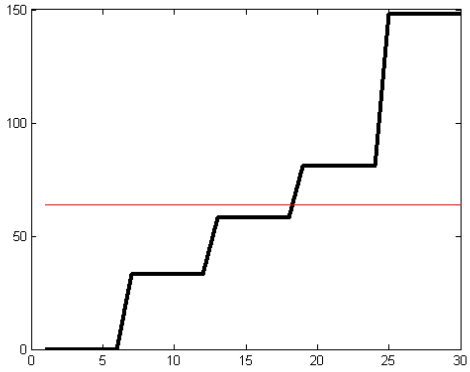

a. SC=5000, over-generalized: all inputs produce a value of 64 ppm (the statistical average of the spiking values).

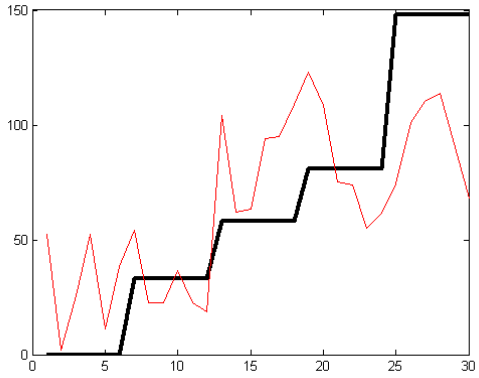

b. SC=500, noisy, but major trend starting to show across data

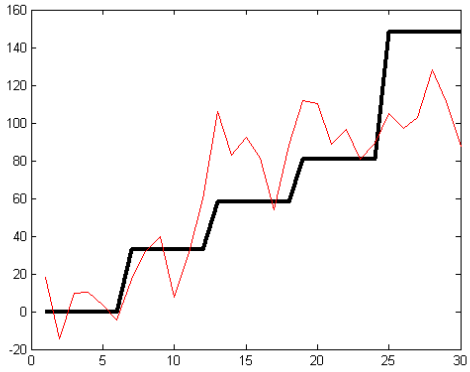

c. SC=50, improving, average error dropping, but still local (concentration-specific) high error.

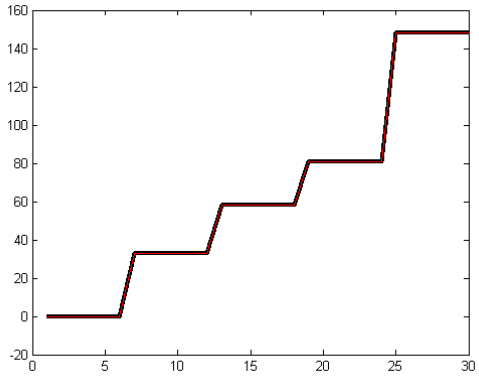

d. SC=5, complete "fit" with zero error between result and target values

Figure 19. Spread Constant Influence on Estimation Error

A wide range of values for EG and SC produced nearly identical results making the computed default values acceptable and the methodology more rigorous. A scatter plot of the target vs. estimated responses for the WBO sensor for acetaldehyde is shown in Figure 20. Each of the six points for each concentration value was obtained by using five of the voltammogram sextuples to predict the sixth one. The procedure was repeated for each of the six voltammograms. Such scatter plots were repeated for all target gases. The plots for all target gases exhibit a linear behavior of target vs. estimated response, but also show significant "open" areas in what would be the calibration curve. To characterize the final instrument, additional concentration measurements should be performed to fill the gaps in the open areas, so that there is uniform confidence in instrument's performance over a wide envelope of concentrations.

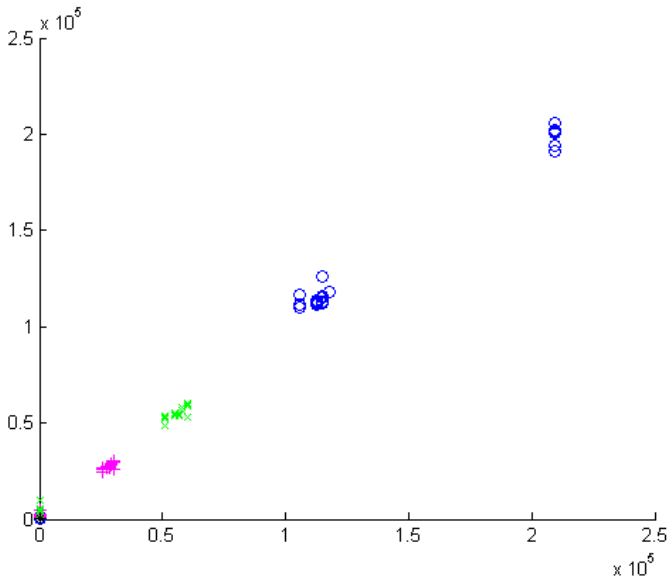

Figure 20. Scatter plot of *predicted* vs. *actual* values for spiking concentrations of 0, 33, 58, 81, and 148 ppm acetaldehyde to diesel exhaust

When presented with voltammograms for air and nitrogen (absolute concentration of acetaldehyde assumed = 0 ppm) the trained GRNN estimator outputted an average "spike" value of -0.6 ppm, which is zero to within the estimation error.

It is apparent from the figures that the GRNN implementation performs as expected, but also that there is room for improvement. The sextuples of voltammogram signatures each show quite low sample-sample drift or error, which actually reduces the GRNN's ability to "generalize" a curve fit as it is reinforced by nearly-identical samples vs. being better generalized by a wider variety of concentration samples. Future more purposeful systems employing this method will use more concentration values for spiking and will actually introduce a small amount of random error (noise) into the sextupled training voltammograms (patterns) and values (targets) to better prevent "memorizing" behavior in favor of better generalization. The wide range of the spiking concentrations that were represented by so few samples also made the curve fitting difficult. A major strength of the voltammetry detection method is its scalability to a wide range of concentration values without saturation of responses. This strength would also be better supported by a larger, more representative set of spiking values for each component.

Analyzing Compositions - CNNS

After the analysis of single gases was implemented using GRNN, the diesel exhaust was analyzed by GC/MS and the actual values for each of the four gases of interest were all found to be less than 1 ppm. With this information, a second GRNN was designed and used to analyze the waveforms and produce measurement values. Most neural networks can perform classifications or analyses. "Classification" accepts an input vector (for this application a voltammogram) and assigns it to a category. "Analysis", or function approximation, accepts a vector input as a set of variable coefficients and produces one or more analog values that represent a functional relationship between the variables and the resultant output. The analysis

type computational neural network effectively maps a function in a way similar to the earlier effort, with the difference being that now there are no unknowns in the training set, and so a direct mapping from voltammogram values to absolute concentrations can be made where earlier only relative (spiked) concentrations could be estimated. All the values in raw diesel exhaust in the tables were set to "0" as a detection threshold, and a GRNN was again designed and trained using the rest of the acetaldehyde-spiked data/sensor WBO 7 responses. Since this was still a very sparse data set, there was some experimentation with training to establish individual interpolation and extrapolation performances.

Curve fits routinely interpolate better than they extrapolate, so training tests were completed to exercise both of these capabilities. The interpolation test removed the 58 ppm spiked voltammograms patterns and concentration targets from the training, then used them as "unknowns" to test the behavior of the partially trained network. The results are shown in Figures 21 and 22.

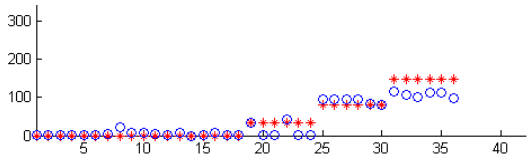

Figure 21. Target concentrations in red, actual results in blue for the post-training processing of the original training pattern set without the 58 ppm acetaldehyde training pattern

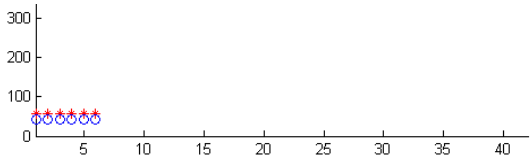

Figure 22. Target concentrations in red, actual results in blue for the *interpolation* validation processing of the removed 58 ppm acetaldehyde training pattern

The extrapolation test removed the 33 ppm spike from the training and then used it as an unknown. Those results are shown in Figures 23 and 24.

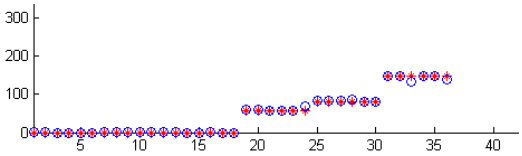

Figure 23. Target concentrations in red, actual results in blue for the post-training processing of the original training pattern Set without the 33 ppm acetaldehyde training pattern

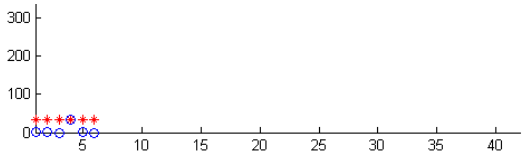

Figure 24. Target concentrations in red, actual results in blue for the *extrapolation* validation processing of the removed 33 ppm acetaldehyde training pattern

The overall results of these first tests were very good. They clearly showed that a wide range of concentrations can be measured for the components and that the average error for a prediction was less than 5%.

For each concentration value, the entire sextuplet of voltammograms was used for training. The GRNN structure and training method allow for a near-zero error over the training set, so there was no advantage in training with only a fraction of the sample set and retaining the rest for validation. Figures 25 through 32 show the revalidation performance of GRNNs trained for each of the four gases of interest. The red stars indicate the target concentration values, and the blue

circles indicate the estimated responses for the training values. The error for all examples is extremely low, less than 5%, with actual zero error for most.

Future characterization experiments will employ more points and fill in the response gaps observed by this first set of experiments.

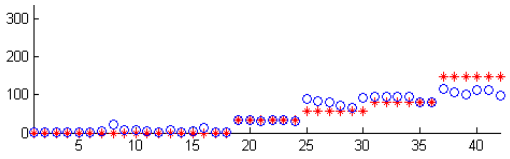

Figure 25. Acetaldehyde WBO 7 revalidation with complete training set

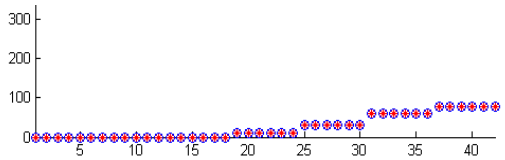

Figure 26. Acrolein WBO 8 revalidation with complete training Set

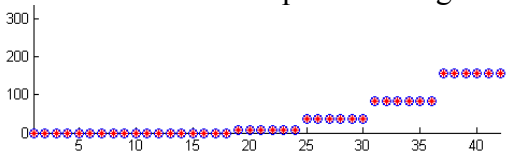

Figure 27. Benzene WBO 8 revalidation with complete training set

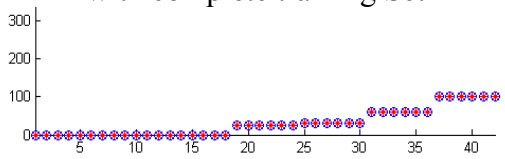

Figure 28. 1,3-Butadiene WBO 8 revalidation with complete training set

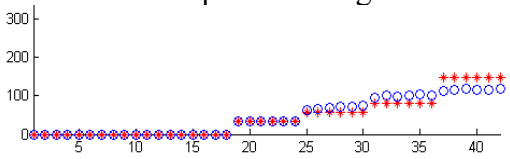

Figure 29. Acetaldehyde YSZ 7 revalidation with complete training set

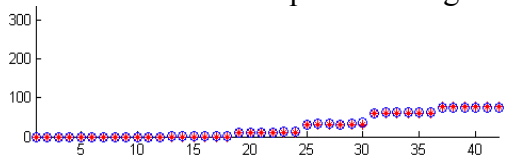

Figure 30. Acrolein YSZ 8 revalidation with complete training set

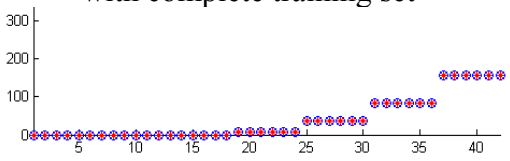

Figure 31. Benzene YSZ 8 revalidation with complete training set

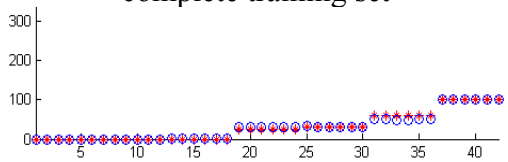

Figure 32. 1,3-Butadiene YSZ 8 revalidation with complete training set

Sensing Instrument Performance Computations

Several different neural algorithms were employed to "reduce" the voltammograms and extract the response contribution from each component in a mixture. Two different GRNN construction strategies were implemented and compared to see which performed better and which was more robust (often simpler). In the first strategy, a single GRNN was trained to extract and produce all of the component values. In the second strategy, a separate analysis GRNN was trained to extract and measure each individual gas component. Both approaches performed similarly as far as analysis and prediction error. Unlike the simple statistical averaging, the value(s) produced by the GRNN do reflect the variable weighting and dominance of portions of the voltammogram where chemical behavior is more closely associated with a given chemical species. In this way, the statistics produced to describe the overall instrument performance are more meaningful if

they include the GRNN reduction of the voltammograms down to single values for each component in a given gas sample.

GRNN Behavior for this Project's Analysis Calculations

During development, training the GRNN under MATLAB is nearly automated. Most operation parameters are computed from architectures and Pattern-Target dimensions. Since the workhorse layer of the GRNN is composed of neurons using a radial basis function (RBF), the controls of that RBF have a large impact on the performance of the overall network. The spread constant (SC) governs how the curve fit function generalizes, or how smooth it is. Figure 33 illustrates the response curve fits for the combined oxygen (O_2), carbon monoxide (CO), carbon dioxide (CO_2), and acetaldehyde (C_2H_4O) analysis example. The error (in arbitrary units) is plotted vertically, the sample number – horizontally. The response curves are dimensioned to fit the voltammograms (100 points → 100 dimensions). Comparison of the target with the actual values in Figure 33 shows (with exaggerated vertical scaling) that both following too closely and smoothing too much are the extreme cases for a curve fit. The displayed curves illustrate the "fit" for each test case, and do not indicate functional relationships.

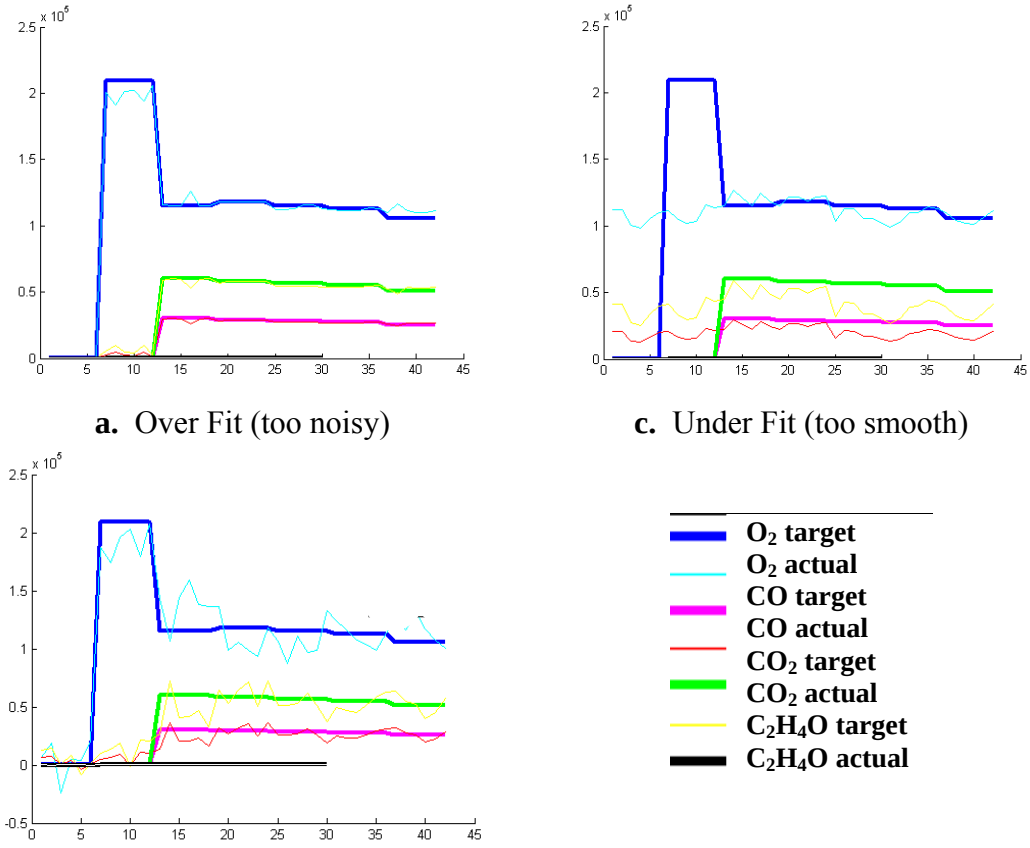

a. Over Fit (too noisy)

c. Under Fit (too smooth)

b. Good Fit

Legend

Figure 33. Estimation Error Impact of the Spread Constant

It should be noted that the curves as displayed in Figure 33 are not meant to indicate functional relationships, but simply illustrate the "fit" at each test case used. The response curves are

dimensioned to fit the voltammograms (100 points → 100 dimensions). These graphs illustrate the error vs. sample point.

Discrimination Results

When complete mixture matrix testing was completed, a GRNN was designed and trained with the sole purpose to identify and differentiate components in various mixtures of the four gases of interest spiked in combinations in a diesel background. This discrimination test was performed to yield analog values as outputs, with gross classification assigned by identification error being less than 25% in any one gas. Overall classification error was significantly less than this, closer to a fraction of a percent for any gas singly or in mixtures. This low error was a function of interference elimination using a combined signal from both YSZ and WBO elements in the sensing array. This was a first time test for this technique with these gases, and further improvements are expected.

Discrimination Capabilities of Sensor Array

A subset of tests exposed the WBO element to varying combinations (pairs and triples) of the four spiking gases, each at a nominal 100 ppm concentration. These tests were designed to establish the initial discrimination capability of the WBO element of the dual-sensor array. The WBO sensors were developed several years earlier by "doping" the YSZ solid electrolyte with tungsten bismuth oxide. This was intended to suppress many of the hydrocarbon reactions, leaving more subtle reactions at the same reaction potentials more visible. The WBO also provided lattice sites for other reactions (such as CO_2) that were less susceptible to YSZ alone. Examination of the WBO error vs. sample number chart clearly shows very low, but not uniform, error, far below what is needed for 100% correct classification of each sample (any error less than 50% would still classify properly).

A second portion of the tests was designed to establish the initial discrimination capability of the YSZ element of the dual-sensor array. The YSZ sensors were the original ANL voltammetric devices and when paired with the standard catalytic platinum working electrode, triggered reactions for a wide range of gas species across a wide range of potentials. Those reactions can readily be observed in Figure 34. In this figure, the gross detected value for each of the spiked gases is shown below the table matrix describing what was in each mixture. The first column on the left, in the upper table and in the lower chart, shows zero spiking for any gas. The upper chart indicates the WBO element gross estimate of component concentration and the lower chart indicates the YSZ element response.

	N2	Air	|---------- diesel spiked with 100 ppms of groups ----------|													
	1-6	7-12	13-18	19-24	25-30	31-36	37-42	43-48	49-54	55-60	61-66	67-72	73-78	79-84	85-90	91-96	
C2H4O	0	0	100	0	0	0	100	0	0	100	100	0	100	0	100	100	C2H4O
C3H4O	0	0	0	100	0	0	100	100	100	0	0	0	100	100	100	0	C3H4O
C6H6	0	0	0	0	100	0	0	0	100	100	0	100	100	100	0	100	C6H6
C4H6	0	0	0	0	0	100	0	100	0	0	100	100	0	100	100	100	C4H6

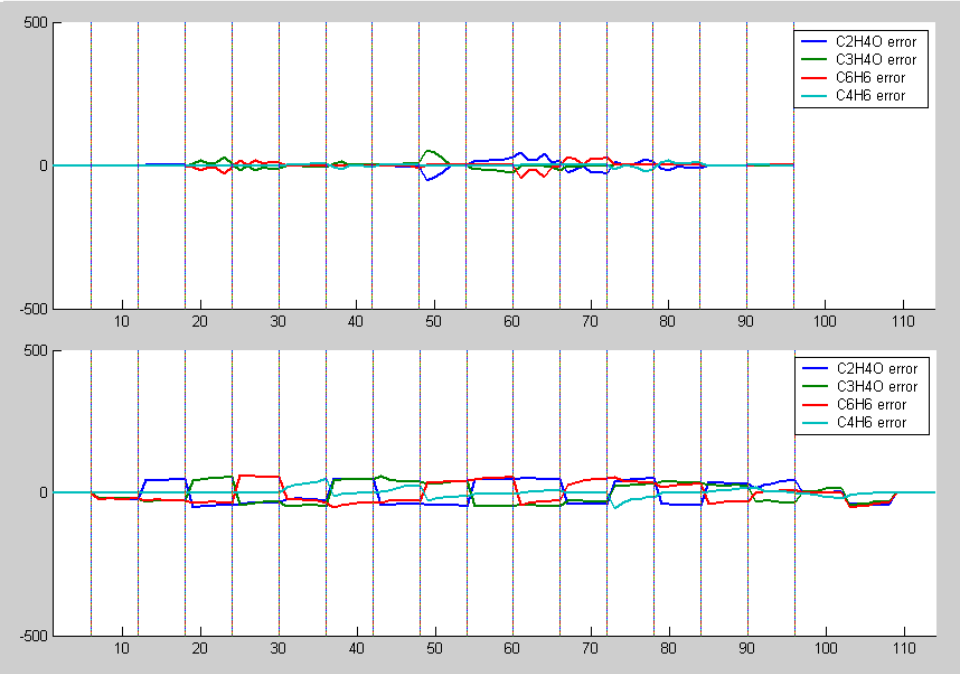

Figure 34. Discrimination Error for Tests 5 and 6, WBO and YSZ Sensors
Note: The upper graph is the WBO response, the lower graph is the YSZ response

For discrimination tests, the error shown for either sensor did not affect gross classification and identification. It is important to note that there is still significant interference between some gas components for this test with the YSZ sensor. Comparing the YSZ error across the chemical compositions against the WBO sensor shows that at the locations where the YSZ sensors (sixth column) exhibits the most interference (large error), the WBO sensors exhibit very low error for the same gas component. This is exactly why the two sensor types were paired and why the discrimination tests were executed with both sensors simultaneously. This complimenting behavior is observed throughout the series of mixture tests.

The average error results across the entire tested concentration range and component combinations are shown in the Table 5. The units of the values reported are ppm. This was a first generation discrimination test for these compounds; the sensors were paired and operated simultaneously. These results are considered gross, and as such, clearly show that with gas concentrations of 100 ppm for all the tests, the average error is similar for all gases and is acceptably low. (The small negative values are typical of these numerical methods and reflect the statistical error inherent in approximation methods. More comprehensive and exhaustive calibration at lower concentration levels will remove this error and inhibit reporting negative physical concentration amounts.)

Table 5. Average Discrimination Error

		Test 5 WBO	Test 6 YSZ	Average % Error
C_2H_4O	acetaldehyde	0.0513	-1.2693	0.609
C_3H_4O	acrolein	0.2661	-1.9638	0.848
C_6H_6	benzene	-0.1952	-1.0578	0.626
C_4H_6	1,3-butadiene	-0.0535	0.4656	0.259

This is a simple average of the gross, un-normalized raw voltammograms, and does not represent the actual lower limit of discrimination capability. Discrimination capability will continue to be improved as more data are gathered and appropriate pre-processing techniques are developed and applied.

The software development plan requires significant data to be gathered and characterization and performance generalized before determining what pre-processing will be required. Several techniques have been successfully applied in the past to improve discrimination by producing a "differential" voltammogram by comparing each sample voltammogram to either a nitrogen gas sample or to a simultaneous "reference" gas sample created on-the-fly by passing a portion of the sample through a tenex trap. Tenex traps effectively remove all organic constituents leaving background air. This technique is not difficult, but does increase the complexity of the process.

Conclusions

Results from these investigations demonstrated that the instrument could be used to detect and discriminate the four gases of interest at low ppm concentrations. *Detection* of the target diesel exhaust gases - acetaldehyde, acrolein, benzene, and 1,3-butadiene - to a 1 ppm limit (to within one standard deviation) was clearly achievable, when these gases occurred singly in a diesel exhaust matrix. Testing also demonstrated that the experimental CEM instrument can *discriminate* between different concentrations of these gases in a diesel exhaust matrix (to within a standard deviation) at concentrations of 1, 5, 10, and 50 ppm. Even the two gases, benzene and acrolein, which exhibit voltammograms in diesel exhaust that look similar to the YSZ sensor, are readily distinguishable using a composite YSZ/WBO array response and [neural network] pattern recognition and approximation algorithms.

The microsensors created in this research could readily be tailored for detection of other industrial chemicals also at part per million levels. Additional effort is needed to improve the sensing for low part per billion level detection. That effort may include the use of a gas pre-concentrator, increasing the effective surface area of the sensors (thus increasing sensitivity), and introducing the use of nanoparticle films (to increase interaction with the gases) to replace the microparticle films used now.

Projects prior to this SERDP effort explored other applications where ppb levels of detection were not required. These included the detection of insect pest (termite) infestations, detection and classification of fires on board naval ships, and detection and classification of toxic gases (cyanide compounds, TICs). The significant advancement of this sensing technology made during the course of this project will allow all of these applications to be readdressed and reasonably solved. Demonstrations of that capability are underway at the time of this report.

References

Bard, Allen J., L.R. Faulkner, 1980. *Electrochemical Methods*, John Wiley & Sons, Inc, New York, NY, 232-236.

Beebe, K.R., R.J. Pell, and M.B. Seasholtz, 1998. *Chemometrics A Practical Guide*, John Wiley & Sons, Inc., New York, NY, 3-332.

Buechler, K., R. D. Noble, C. A. Koval, and W.A. Jacoby, 1999. "Investigation of the effects of controlled periodic illumination on the oxidation of gaseous trichloroethylene using a thin film of TiO_2," *Ind. Eng. Chem. Res*. Vol. 38:892-896.

Burges, C.J.C., 1998. "A Tutorial on Support Vector Machines for Pattern Recognition," *Data Mining and Knowledge Discovery* Vol. 2, No. 2:121-167.

Butler, E.C. and A. P. Davis, 1993. "Photocatalytic oxidation in aqueous titanium dioxide suspensions: the influence of dissolved transition metals," *J. Photochem. Photobiol. A: Chem*. Vol. 70:273-283.

Carotta, M.C., G. Martinelli, L. Crema, M. Gallana, M. Merli, G. Ghiotti, E. Traversa, 2000. "Array Of Thick Film Sensors For Atmospheric Pollutant Monitoring," *Sensors and Actuators B-Chemical* Vol. 68:1-8.

Carotta, M.C., M. Ferroni, D. Gnani, V. Guidi, M. Merli, G. Martinelli, M.C. Casale, M. Notaro, 1999. "Nanostructured Pure And Nb-Doped Tio2 As Thick Film Gas Sensors For Environmental Monitoring," *Sensors and Actuators B-Chemical*, Vol. 58, No. 1-3:310-317.

Comini, E., G. Sberveglieri, V. Guidi, 2000. "Ti-W-O Sputtered Thin Film As N- Or P-Type Gas Sensors," *Sensors and Actuators B-Chemical* Vol. 70, No. 1-3:108-114.

Compilation of Air Pollutant Emission Factors, AP-42, Fifth Edition, Volume I: Stationary Point and Area Sources, 1995. U.S. EPA Report AP-42, <http://www.epa.gov/ttn/chief/ap42/index.html>

d'Hennezel, O. and D. F. Ollis, 1997. "Trichloroethylene-promoted photocatalytic oxidation of air contaminants," *J. of Catalysis* Vol. 167:118-126.

d'Hennezel, O., P. Pichat, and D. F. Ollis, 1998. "Benzene and toluene gas-phase photocatalytic degradation over H_2O and HCl pretreated TiO_2: by-products and mechanisms," *J. Photochem. Photobiol. A: Chemistry* Vol. 118:197-204.

Dai, G.R. 1998. "A Study of the Sensing Properties of Thin Film Sensor to Trimethylamine," *Sensors and Actuators B-Chemical* Vol. 53:No. 1-2:8-12.

Das, S., M. Muneer, and K.R. Gopidas, 1994. "Photocatalytic degradation of wastewater pollutants. Titanium-dioxide-mediated oxidation of polynuclear aromatic hydrocarbons," *J. Photochem. Photobiol. A: Chem*. Vol. 77:83-88.

Edelman, F., H Hahn, S. Seifried, C. Alof, H. Hoche, A. Balogh, P. Werner, K. Zakrzewska, Radecka, M;Pasierb, P. Chack, A. Mikhelashvili, V. Eisenstein, G., 2000. "Structural Evolution Of SnO_2-TiO_2 Nanocrystalline Films For Gas Sensors," *Materials Science and Engineering B-Solid State Materials for Advanced Technology* Vol. 69:386-391.

Edmonds, T.E., editor, 1988. *Chemical Sensors*, Blackie and Son Ltd, New York, NY.

FDM, 2003. Engineering notes about Fused Deposition Modeling from the Prototype 3D company, <http://www.prototype3d.com/prototypeb.html>

FDM, 2003. Engineering notes about Fused Deposition Modeling from the Stratasys Corporation, <http://www.stratasys.com/NA/index.html>

Fraden, Jacob, 1993. *AIP Handbook of Modern Sensors, Physics, Designs, and Applications*, American Institute of Physics, New York, NY, 532-546.

Freeman, J., D. Skapura, 1991. *Neural Networks, Algorithms, Applications, and Programming Techniques*, Addison-Wesley Publishing Company, reading, MA, 89-111.

Garzella, C., E. Comini, E. Tempesti, C. Frigeri, G. Sberveglieri, 2000. "TiO_2 Thin Films By A Novel Sol-Gel Processing For Gas Sensor Applications," *Sensors and Actuators B-Chemical* Vol. 68:No. 1-3:189-196.

Golego, N., S. A. Studenikin, and M. Cocivera, 2000. "Sensor photoresponse to thin-film oxides of zinc and titanium to oxygen gas," *J. Electroanalytical Society* Vol. 147:1592-1594.

Hager, S. and R. Bauer, 1999. "Heterogeneous photocatalytic oxidation of organics for air purification by near UV irradiated titanium dioxide," *Chemosphere* Vol. 38:1549-1559.

Henrich, V.A., and P.A. Cox, 1994. *The Surface Science of Metal Oxides*, Cambridge University Press, Cambridge, New York.

Islam, M.R. N. Kumazawa, M. Takeuchi, 1998. "Titanium Dioxide Chemical Sensor Working With AC Voltage," *Sensors And Actuators B-Chemical* Vol. 46, No.2:114-119.

Jacoby, W., M.R. Nimlos, D. M. Blake, R. D. Noble, and C. A. Koval, 1994. "Products, intermediates, mass balances, and reaction pathways for the oxidation of trichloroethylene in air via heterogeneous catalysis," *Environ. Sci. Technol*. Vol. 28:1661-1668.

Joo, B.S., N.J. Choi, Y.S. Lee, J.W. Lim, B.H. Kang, and D.D. Lee, 2001. "Pattern Recognition of Gas Sensor Array Using Characteristics of Impedance," *Sensors and Actuators B-Chemical* Vol. 77, No. 1-2:209-214.

Kumazawa, N., M. R. Islam, and M. Takeuchi, 1999. "Photoresponse of a titanium dioxide chemical sensor," *J. Electroanalytical Chemistr* Vol. 472:137-141.

Luo, Y. and D. F. Ollis, 1996. "Heterogeneous photocatalytic oxidation of trichloroethylene and toluene mixtures in air: kinetic promotion and inhibition, time-dependent catalyst activity," *J. Catalysis* Vol. 163:1-11.

Maira, A. J., K. L. Yeung, Y. Lee, P.L. Yue, and C.K. Chan, 2000. "Size effects in gas-phase photo-oxidation of trichloroethylene using nanometer-sized TiO_2 catalysts," *J. of Catalysis* Vol. 192:185-196.

Marcelloni, F., 2001. "Recognition of Olfactory Signals Based on Supervised Fuzzy C-Means and K-NN Algorithms," *Pattern Recognition Letters* Vol. 22, No. 9:1007-1019.

Masters, T., 1993. *Practical Neural Network Recipes in C++*, Academic Press, Inc, Boston, MA, 174-185.

MATLAB Curve Fitting Toolbox User's Guide, 2001. The MathWorks Inc., Natick, MA.

MATLAB Documentation Set (ver 6), 2003. MathWorks, Inc., Natick, MA.

Meshkov, N.K., L.R. Skubal, T. Rajh, and M.C. Thurnauer, 1999. "Removal of Heavy Metals from Aqueous Waste Streams Using Surface-Modified Nanosized TiO_2 Photocatalysts," *J. Adv. Oxid. Technol.* Vol. 4:174-178.

Meshkov, Natalia, L. Skubal, and M.C. Vogt, 2003. "An Interim Report Describing ANL Testing Results", *The Development of Spatially-Based Emission Factors From Real-Time Measurements of Gaseous Pollutants Using Cermet Sensors - SERDP Project CP-1243*, Argonne National Laboratory, prepared for SERDP, November.

Neural Networks Toolbox Users Guide (ver 4), 2003. MathWorks, Inc., Natick, MA.

Noguchi, T. and A. Fujishima, 1998. "Photocatalytic degradation of gaseous formaldehyde using TiO_2 film," *Environ. Sci. Technol* Vol. 32:3831-3833.

Pelckmans, K., J.A.K. Suykens, T. Van Gestel, J. De Brabanter, L. Lukas, B. Hamers, B. De Moor, and J. Vandewalle, 2003. *LS-SVMlab Toolbox User's Guide, version 1.5*, Technical Report 02-145, Department of Electrical Engineering, ESAT-SCD-SISTA, Katholieke Universiteit Leuven, Leuven-Heverlee, Belgium, February.

Radomski, R., M. Radomska, M., Dankowski, K. Szajowska, and Z. Wisialski, 1995. "Microcomputer-Controlled Electrochemical Universal Meter", *Computer and Chemistry* Vol. 19, No. 3:303

Raimundo, I.M., and R. Narayanaswamy, 2001. "Simultaneous Determination of Relative Humidity and Ammonia in Air Employing an Optical Fibre Sensor and Artificial Neural Network", *Sensors and Actuators B – Chemical* Vol. 74, No. 1-3:60-68.

Salikhdzhanova, R. M.-F., A. I. Gorobets, and N. Ya. Petrova, 1994. "Automation of Polarographs and Voltammetric Analyzers", *Measurement Techniques* Vol. 37, No. 7:835-838.

Sampath, S., H. Uchida, and H. Yoneyama, 1994. Photocatalytic degradation of gaseous pyridine over zeolite-supported titanium dioxide," *J. of Catalysis* Vol. 149:89-194.

Sberveglieri, G. E. Comini, G. Faglia, M.Z. Atashbar, W. Wlodarski, 2000. "Titanium Dioxide Thin Films Prepared For Alcohol Microsensor Applications," *Sensors and Actuators B-Chemical* Vol. 66, No. 1-3:39-141.

Schölkopf, B., K. Sung, C.J.C. Burges, F. Girosi, P. Niyogi, T. Poggio, and V. Vapnik, 1997. "Comparing Support Vector Machines with Gaussian Kernels to Radial Basis Function Classifiers," *IEEE Transactions on Signal Processing* Vol. 45:No. 11:2758-2765.

Serpone N., E. Pelizzetti, 1989. *Photocatalysis Fundamentals and Applications*, John Wiley and Sons, Inc., New York.

Sharma, R.K.; M.C. Bhatnagar, and G.L. Sharma, 1996. "Effect of Nb Metal Ion in TiO_2 Oxygen Gas Sensor," *Applied Surface Science*, Vol. 92:647-650.

Signal Processing Toolbox Users Manual, (ver 6), 2001. The MathWorks, Inc., Natick, MA.

Sirisuk, A., C.G. Hill, Jr., and M. A. Anderson, 1999. "Photocatalytic degradation of ethylene over thin films of titania supported on glass," *Catalysis Today* Vol. 54:159-164.

Skubal, L.R. 1999. "Removal of Lead, Copper, and Cadmium from Water Using Surface-Enhanced Titanium Dioxide Colloids," Ph.D. Thesis, The Pennsylvania State University.

Skubal, L.R. and N.K. Meshkov, 1996. "Photocatalytic Removal of Heavy Metals from Aqueous Waste Streams," *Women's Second Technical Symposium -Proceedings of Argonne National Laboratory*, April 29-30.

Skubal, L.R., N.K. Meshkov, T. Rajh, and M.C. Thurnauer, 2000. "Cadmium Removal from Water Using Thiolactic Acid-Modified Titanium Dioxide Nanoparticles," *J. Adv. Oxid. Technol* in press.

SLA, 2004. Stereolithography engineering notes from the Vistatek Corporation, <http://www.vistatek.com/stereo.html>

Smyth, Malcom R., and J. G. Vos, 1992. *Comprehensive Analytical Chemistry-Analytical Voltammetry, Vol XXVII*, Wilson and Wilson, Elsevier Science Publishing Company Inc., New York, NY, 20, 34, 59.

Sopyan, I., S. Murasawa, K. Hashimoto, and A. Fujishima, 1994. "Highly efficient TiO_2 film photocatalyst. Degradation of gaseous acetaldehyde," *Chemistry Letters* 723-726.

Stern, A.C., ed., 1968. *Air Pollution Vol.III Sources of Air Pollution and Their Control*, Academic Press, New York.

Stetter, J.R., W.R Penrose, S. Zaromb, and A.F. Cohen, 1984. *Feasibility of Developing Low-Power, Low-Current Methane Sensors for the Intrinsically Safe Mine Monitoring System*, Argonne National Laboratory, Argonne, IL, ANL/ES-138, 6.

Takeda, N., T. Torimoto, S. Sampath, S. Kuwabata, and H. Yoneyama, 1995. "Effect of inert supports for titanium dioxide loading on enhancement of photodecomposition rate of gaseous propionaldehyde," *J. Phys. Chem*. Vol. 99:9986-9991.

Traversa, E., Y. Sadaoka, M.C. Carotta, G Martinelli, 2000. "Environmental Monitoring Field Tests Using Screen-Printed Thick-Film Sensors Based On Semiconducting Oxides," *Sensors and Actuators B-Chemical* Vol. 65, No. 1-3:181-185

Winquist, F, E.G. Hornsten, H. Sundgren, and I. Lundstrom, 1993. "Performance of an Electronic Nose for Quality Estimation of Ground Meat," *Measurement Science and Technology* Vol. 4, No. 12:1493-1500.

Appendices

Appendix A

Comprehensive Experimental Data

The data generated during the course of this project is substantial, and it is not practical or useful to reproduce the actual data in table form. The entire collection of experimental plans, spreadsheets, acquired measurements, charts, and software code are available on a CDROM accompanying the original copy of this report.

Appendix B

List of Technical Publications

We have a patent application pending for the TiO_2 sensor.

Poster Abstract for Partners in Environmental Technology Technical Symposium and Workshop, Washington, D.C. December 2-4, 2003.

The Department of Defense needs to identify and characterize emissions of trace air toxic compounds, especially persistent organic pollutants, from operations/activities at its facilities. Currently, the available ambient air toxic concentration data are non-temporal and non-spatial, and produce low-quality emission prediction factors that must often significantly overestimate the emissions produced. This project is developing a new emissions characterization technique to produce "instantaneous" pollutant concentration profiles of emissions from both stationary and mobile sources. The technique will combine experimental electronic nose instrument and a spatial-temporal emissions model. The miniature instrument employs several types of cermet microsensors, experimental photocatalytic sensors, and more mature voltammetric sensors. The approach will be developed and validated focusing on gases from diesel exhaust, specifically, benzene, 1,3-butadiene, acetaldehyde, and acrolein. Interim results are presented. They include sensor responses from diesel component gases at multiple concentrations, individually and in combinations and in air.

Appendix C

Computational Neural Networks Used for Chemometrics

A neural network is inspired by and loosely models the architecture and information processing capability of the biological brain (Masters 1993). An Artificial Neural Network (ANN) accomplishes this by simulating each biological neuron with an integrated circuit as a collection of gates and transistors while a Computational Neural Network (CNN) accomplishes this through execution of a series of computer instructions. Neural networks can be structured to perform classification (Raimundo 2001), to approximate equations (Joo et al. 2001), and to predict values (Freeman 1991, Winquist 1993).

Several different models for neurons are available; each supports a different range of network architectures and artificial learning methods. A generalized neuron model includes some input stage with variable weighted interconnections to the outputs of other neurons, a summation/comparison stage for combining the weighted inputs, a transfer function that reduces the information passed along through the neuron, an output stage that connects to the inputs of other neurons, and some feedback/training method to adjust the weights so that a desired output is produced when exposed to known inputs. Some network architectures require an optional delay stage to support adaptive learning.

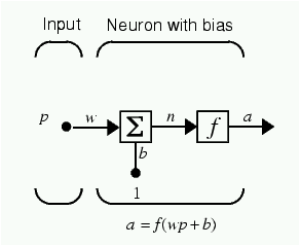

Figure C1. Generalize Neuron Model

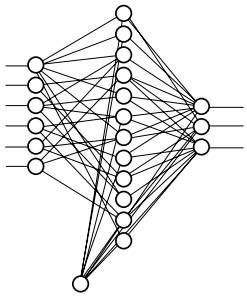

Figure C2. Layers Combined into a Network

Generalized network architecture includes an input layer that interfaces directly to the sensor signals, a hidden layer that reduces information and makes intermediate choices and performs feature extraction, and an output layer that selects intermediate answers and provides the classification or component analysis information (MATLAB, Neural Net Toolbox). In a generic architecture, neurons are referred to as nodes, and inter-node connections are only made between adjacent layers.

Electronic noses generally pursue composite odor classification, with component analysis representing a more difficult secondary goal. Probabilistic neural network (PNN) classifiers are the most popular CNNs used with electronic noses. They duplicate the functionality of K-nearest neighbor or Bayesian statistical classifiers, though the NN versions often out-perform both (Stetter et al. 1993). The PNN uses a radial basis function neuron and competitive hidden layer network architecture. PNNs require supervised training where a set of inputs is constructed that has predetermined desired outputs (categories). During training, a new neuron is constructed for each sample in the training set. The weights between the inputs and the competitive neuron are copies of the input values themselves. The output of each neuron goes to

a matching category in the final competitive output layer. Multiple examples of a given input/output pairing create additional copies of a neuron and strengthen the possibility of selection for that category, reflecting statistical probabilities of that category's occurrence in a population, hence the name "probabilistic" neural network.

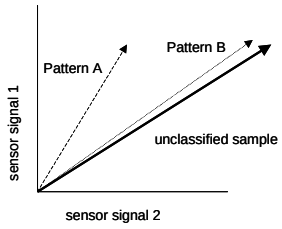

Figure C3. Vector Comparison

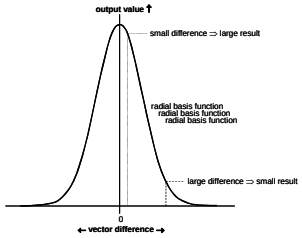

Figure C4. Radial Basis Function

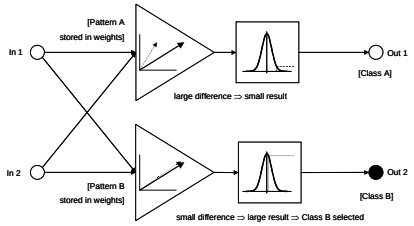

Figure C5. PNN Layers

During operation of a PNN, a vector containing the input values is presented to each neuron in the input layer. Each neuron compares the input vector and the vector formed from its own local set of weights by computing a Cartesian distance between the vectors. Internal to each neuron the distance is then passed through the local radial basis transfer function (a Gaussian bell curve centered on input = 0 to produce an output = 1) that outputs a high value for small distances (differences) and very small values for larger distances. The result is that the neuron whose weights most closely match the input vector produces the highest final output value and the output layer assigns the input to that category. The options for training PNNs vary with trade-offs between flexibility, memory resource use, and speed of training.

A common misconception of neural networks is that they have to remain black boxes and that internal behaviors are too complex to allow inspection, review, and rigorous analysis. This criticism can be avoided if the network (such as a PNN) structure is kept simple and a fixed-length vector-type input is adopted. Simple NNs do not lose their performance benefits, are coded easily in software and firmware, and can be optimized for a given application.

For this stage of instrument development, analyses networks that produce analog values were developed, as detection limits and discrimination capabilities required measures of performance that classifying networks would mask. Future applications may still change this, when diesel sources may be better monitored by classifying the levels and ratios of their outputs vs. measuring for specific threshold crossings.

General Regression Neural Networks

The GRNN was implemented using MathWorks™ MATLAB Version 6.5.0.180913a (R13) and the Neural Network Toolbox ver. 4.0.2. A generalized regression neural network (GRNN) is

often used for function approximation (MathWorks 2003). The general GRNN architecture has a radial basis hidden layer and a special linear output layer as shown below (Figure C6).

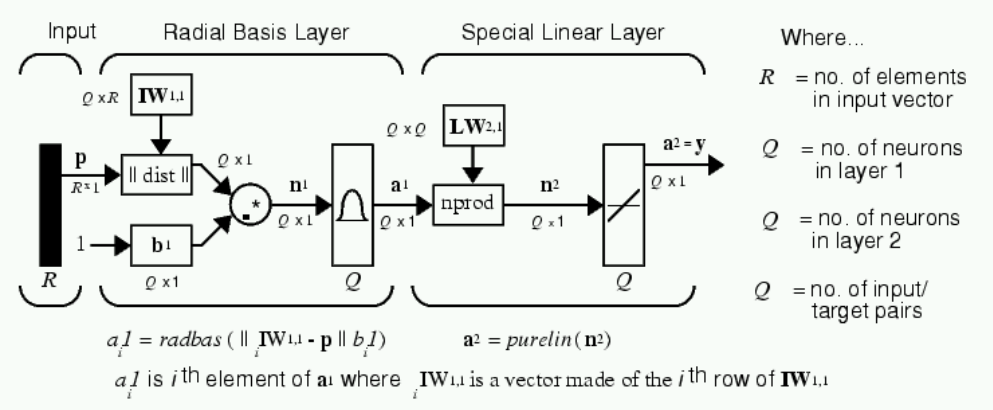

Figure C6. Architecture for General Regression Neural Networks

The first layer has as many neurons as there are input-target vector pairs in the training pattern set P. The bias b1 is set to a column vector of 0.8326/SPREAD. The user chooses SPREAD (or SC), the distance an input vector must be from a neuron's weight vector to be 0.5. Each neuron's weighted input is the distance between the input vector and its weight vector, calculated with *dist*. Each neuron's net input is the product of its weighted input with its bias, calculated with *netprod*. Each neurons' output is its net input passed through *radbas*. If a neuron's weight vector is equal to the input vector (transposed), its weighted input will be 0, its net input will be 0, and its output will be 1. A larger spread leads to a large area around the input vector where layer 1 neurons will respond with significant outputs. Therefore if spread is small the radial basis function is very steep so that the neuron with the weight vector closest to the input will have a much larger output than other neurons. The network will tend to respond with the target vector associated with the nearest design input vector. As spread gets larger the radial basis function's slope gets smoother and several neurons may respond to an input vector. The network then acts like it is taking a weighted average between target vectors whose design input vectors are closest to the new input vector. As spread gets larger more and more neurons contribute to the average with the result that the network function becomes smoother. The linear output layer allows the network to produce smooth continuous values for outputs, lending to good behavior as a general function approximator. All radial basis networks, including the GRNN, train very quickly and reproducibly and make for dependable components in an instrument.

Appendix D

Support Vector Machines Evaluated for Chemometrics

Classical algorithms like the least squares-support vector machine (LS-SVM) employ a functional "kernel" to identify "features" in the data (Schölkopf et al. 1997). Features are local sample point-to-sample point relationships which then taken together, amount to a pattern over the larger dataset. SVM formulation embodies the Structural Risk Minimization (SRM) principle, as opposed to the Empirical Risk Minimization (ERM) approach commonly employed within other statistical learning methods (Burges 1998). SRM minimizes an upper bound on the generalization error, as opposed to ERM which minimizes the error over the training data itself (Pelckmans et al. 2003). It is this difference which equips SVMs with a greater potential to generalize, and to do so with fewer model samples for each class, or each regression state. SVM methods identify the key "support vectors" that lie along and define the buffered boundaries of the classes in a classification problem, and which separate definable states in a functional regression problem. These support vectors are then used for comparisons for class assignment or for weighted influence in regression analysis. The remainder of the training sample vectors (signatures) are effectively ignored and can be eliminated from the processing leaving behind a simpler, more generalized algorithm.

Performance on synthetic data

Since the GRNN and PNN methods produced no classification error over the training sets, no improvement via the SVMs was anticipated. Sample problems were constructed to compare SVM regression methods to the GRNN approximation performed earlier. Pre-tested LS-SVM code for MATLAB was obtained and used to model several types of functions. The SVM algorithms were compared directly to the same RBFN and GRNN algorithms used to analyze the voltammetry signature data. The results shown below in Figures D1 through D4 indicate that the properly tuned RBFN and GRNN perform as well as the SVM over these problems.

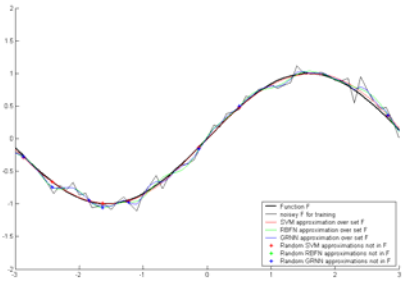

Figure D1. Approximations of a Sine Function

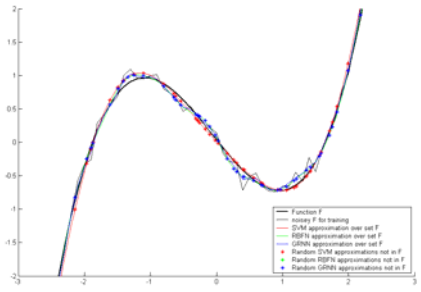

Figure D2. Approximations of a Polynomial Function

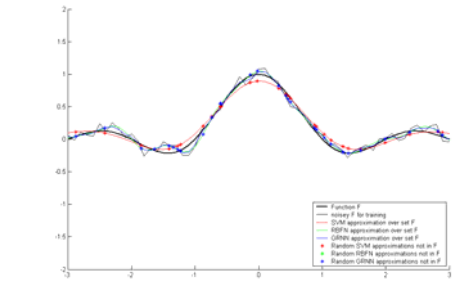

Figure D3. Approximations of a Sinc Function

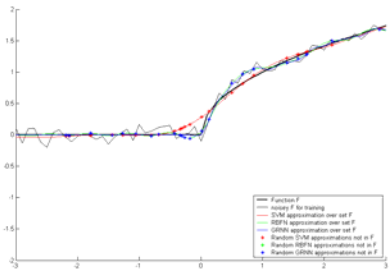

Figure D4. Approximations of a Square root Function

Comparison of RBFN, GRNN, and SVM Function Approximation Methods for Common Functions

Appendix E

The MATLAB Development Environment

MATLAB was selected as a development environment for the instrument for several reasons. Software tools exist to significantly streamline complete instrument and system development, including the Excel Builder, Curve Fitting Toolbox, Embedded Target for Motorola microcontroller, and Neural Network Toolbox.

MATLAB Excel Builder provides the capability to incorporate MATLAB models and functions quickly in Excel worksheets. A graphical user interface enables the user to build and deploy Excel Add-Ins containing functionality designed in MATLAB but accessed from the Excel environment.

The Curve Fitting Toolbox provides a central access point and a graphical user interface (GUI) for the functions the users need to perform applications that involve curve fitting. The toolbox provides routines for preprocessing data, as well as creating, comparing, analyzing, and managing models.

The Embedded Target for Motorola® MPC555 lets the user deploy production code generated from Real-Time Workshop Embedded Coder directly onto the MPC555 microcontroller, a dramatic time-saver when developing dedicated instruments.

The Neural Network Toolbox provides both command line and a GUI interface to a broad collection of neural computing tools and demonstrations. The developed NNs are built with streamlined notation making management of large data sets practicable.

Experimental toolboxes, such as the Least Squares-Support Vector Machine Toolbox, allow the latest data processing methods to be tested.

Any of the MATLAB native m-code application programs can be automatically translated into C for execution outside of MATLAB or on high-speed DSP hardware.

Appendix F.

Rapid Prototyping

Rapid Prototyping (RP) is a term applied to several model fabrication technologies that allow three dimensional computer aided design (CAD) software to control automated machinery and construct parts, complete, in a matter of minutes or hours with little human physical attention [FDM, SLA]. Popular methods were selected for this project's application, to introduce RP into the research and development loop. The materials that were used dictated the fabrication methods employed. Very good mechanical tolerances were achieved by both methods, and three different materials were used to fabricate identical enclosures. It was anticipated that the sensing array that was housed by the enclosure would be exposed to elevated operating temperatures. Many plastics off-gas when heated and the gases produced might interfere with target gas analytes. Future experiments will indicate whether the insides of the enclosures will require chemical resistant linings to be spray coated to eliminate the effects of off-gassing.

Materials

The plastic materials available for RP work includes

- RenShape® SL 5195, a UV-cured clear amber polymer capable of 0.05 mm dimensional resolution with a density of 1.18 g/cc.
- Somos® 9120 Epoxy Photopolymer, a UV-cured transparent amber plastic that is chemical resistant and behaves like polypropylene, chemical resistant with a density of 1.13 g/cc.
- WaterShed™ 11120, a light green tinged plastic that mimics ABS with a density of 1.12 g/cc.
- ABS, a polycarbonate.

SLA – Stereolithography

Stereolithography, or SLA, creates a tangible 3-D object by directing ultraviolet laser radiation onto a vat of polymer resin (liquid plastic). Parts are commonly finish-cured in an ultraviolet oven then hand-polished and finished to specifications. SLA methods work well with epoxies and WaterShed materials.

FDM – Fused Deposition Modeling

During FDM (Fused Deposition Modeling) a temperature-controlled head extrudes ABS or Polycarbonate plastic material, layer by layer. The designed object emerges as a solid three-dimensional part without the need for tooling. A Solid Model 3D design (.STL file) is imported into pre-processing software. The part design is orientated and software slices the 3D drawing into horizontal layers varying from .005" -.014" inch thickness. Support is automatically or custom generated based on the position and geometry of the part. The system operates in X, Y and Z axes. In effect, it draws the model one layer at a time.